AMANDA PATRÍCIA GONÇALVES

PRODUCTION, CHARACTERIZATION AND EVALUATION OF THE CHEMOTHERAPEUTIC AND IMMUNOGENIC POTENTIAL OF PROTEIN-BASED VIRUS-LIKE PARTICLES IN TUMORAL AND IMMUNE CELL LINES

Thesis submitted to the Cellular and Structural Biology Program of the Universidade Federal de Viçosa in partial fulfillment of the requirements for the degree of *Doctor Scientiae*.

Adviser: Anésia Aparecida dos Santos

VIÇOSA – MINAS GERAIS

2023

Ficha catalográfica elaborada pela Biblioteca Central da Universidade Federal de Viçosa - Campus Viçosa

T
G635p
2023

Gonçalves, Amanda Patrícia, 1994-
Production, characterization and evaluation of the chemotherapeutic and immunogenic potential of protein based virus-like particles in tumoral and immune cell lines / Amanda Patrícia Gonçalves. – Viçosa, MG, 2023.
1 tese eletrônica (66 f.): il. (algumas color.).

Texto em inglês.
Orientador: Anésia Aparecida dos Santos.
Tese (doutorado) - Universidade Federal de Viçosa, Departamento de Biologia Geral, 2023.
Inclui bibliografia.
DOI: https://doi.org/10.47328/ufvbbt.2023.755
Modo de acesso: World Wide Web.

1. Células - Mecanismos de controle. 2. Nanotecnologia. 3. Vacinas. I. Santos, Anésia Aparecida dos, 1969-. II. Universidade Federal de Viçosa. Departamento de Biologia Geral. Programa de Pós-Graduação em Biologia Celular e Estrutural. III. Título.

CDD 22. ed. 571.6

Bibliotecário(a) responsável: Euzébio Luiz Pinto CRB-6/3317

AMANDA PATRÍCIA GONÇALVES

PRODUCTION, CHARACTERIZATION AND EVALUATION OF THE CHEMOTHERAPEUTIC AND IMMUNOGENIC POTENTIAL OF PROTEIN-BASED VIRUS-LIKE PARTICLES IN TUMORAL AND IMMUNE CELL LINES

Thesis submitted to the Cellular and Structural Biology Program of the Universidade Federal de Viçosa in partial fulfillment of the requirements for the degree of *Doctor Scientiae*.

.

APPROVED: October 30th, 2023.

Assent:

gov.br Documento assinado digitalmente
AMANDA PATRICIA GONCALVES
Data: 14/12/2023 17:11:57-0300
Verifique em https://validar.iti.gov.br

Amanda Patrícia Gonçalves

gov.br Documento assinado digitalmente
ANESIA APARECIDA DOS SANTOS
Data: 14/12/2023 17:01:14-0300
Verifique em https://validar.iti.gov.br

Anésia Aparecida dos Santos
Adviser

ACKNOWLEDGMENTS

On this acknowledgments page, I kindly ask for permission to do them in my mother language. Before that, I need to express my deep acknowledgement to the Coordenação de Aperfeiçoamento de Pessoal de Nível Superior (CAPES), for research funding and for granting my scholarship. This study was financed in part by the Coordenação de Aperfeiçoamento de Pessoal de Nível Superior – Brasil (CAPES) – Finance Code 001. That said, I will say some words in Brazilian Portuguese from now.

Nesta página dedico meus mais profundos agradecimentos à todas as pessoas e instituições que tornaram possível esse trabalho.

Nomeio especialmente meu companheiro, família, amigos, orientadora, supervisores e psicóloga – pelo suporte emocional;

Deus, anjos da guarda e outras memórias tranquilas – pelo suporte espiritual;

A Universidade Federal de Viçosa, a Wageningen University and Research, os departamentos de Biologia Geral e de Física - UFV e às agências de fomento CAPES, CNPQ e FAPEMIG – pelo suporte físico e financeiro;

Aos governantes progressistas, frequentemente tão atacados – por criar políticas públicas de acesso e permanência na educação superior, algo essencial para a minha entrada e permanência na universidade pública;

E, por fim, agradeço às pessoas brilhantes que promovem a mudança do mundo através da ciência – pela motivação e vontade de continuar produzindo em tempos tão fundamentalistas.

“Coração de estudante
Há que se cuidar da vida
Há que se cuidar do mundo
Tomar conta da amizade

Alegria e muito sonho
Espalhados no caminho
Verdes, planta e sentimento
Folhas, coração, juventude e fé”

(Milton Nascimento)

ABSTRACT

GONÇALVES, Amanda Patrícia, D.Sc., Universidade Federal de Viçosa, October, 2023. **Production, characterization and evaluation of the chemotherapeutic and immunogenic potential of protein-based virus-like particles in tumoral and immune cell lines**. Adviser: Anésia Aparecida Santos.

In this thesis, nanotechnology was used to develop three inedited platforms with clinical applications. Results are presented in three chapters written in article format. In the first chapter, *in vitro* assays are used to characterize a new doxorubicin (DOX) carrier *virus-like* platform and to evaluate the cell effects of murine melanoma cells treated with free DOX or carried DOX. It is showed that carried DOX promotes higher cell death rates and enter cells in a different manner whether compared with free DOX. In the second chapter, the Spy Catcher/Spy Tag technology was used to conjugate different peptides to rod-shaped *virus-like* particles (VLPs). It is shown that two different types of antigen-presenting cells (APCs) can take up decorated VLPs and this promotes the activation of immune response by increasing CD80 and CD86 expression. In the third chapter, Spy Catcher/Spy Tag technology was also used to conjugate anti-EGFR nanobodies to the surface of DOX-loaded VLPs. It is shown that particles displaying anti-EGFR nanobodies promote a more accentuated decrease on cell viability of human colorectal cancer cells whether compared with non-decorated particles. In conclusion, this work present the full production and characterization of three distinct nanoplatforms and a solid *in vitro* evaluation of a range of cell mechanisms such as endocytosis, apoptosis and autophagy. The achieved results suggest that the constructions presented here have features that put them as nanoplatforms with potential clinical applications such as vaccine platforms and drug delivery systems.

Keywords: Nanotechnology. Drug-delivery systems. Vaccine platforms. Protein-based particles. Nucleic acid-based particles. Particle decoration. Doxorubicin. Cancer.

RESUMO

GONÇALVES, Amanda Patrícia, D.Sc., Universidade Federal de Viçosa, outubro de 2023. **Produção, caracterização e avaliação do potencial quimioterapêutico e imunogênico de partículas proteicas virus-like em linhagens de células tumorais imunes.** Orientadora: Anésia Aparecida Santos.

Nesta tese, a nanotecnologia foi utilizada para desenvolver três plataformas inéditas com aplicações clínicas. Os resultados são apresentados em três capítulos escritos em formato de artigo. No primeiro capítulo, ensaios *in vitro* são usados para caracterizar uma nova plataforma *virus-like* carreadora de doxorrubicina (DOX) e para avaliar os efeitos celulares em células de melanoma murino tratadas com DOX livre ou com DOX carreada. É demonstrado que a DOX carreada promove maiores taxas de morte celular bem como entra nas células de maneira diferente se comparada à DOX livre. No segundo capítulo, a tecnologia Spy Catcher/Spy Tag foi usada para conjugar diferentes peptídeos a partículas *virus-like* (VLPs) cilíndricas. É demonstrado que dois tipos diferentes de células apresentadoras de antígenos (APCs) conseguem interiorizar VLPs decoradas e isso promove a ativação da resposta imune através do aumento da expressão de CD80 e CD86. No terceiro capítulo, a tecnologia Spy Catcher/Spy Tag também foi usada para conjugar nanocorpos anti-EGFR à superfície de VLPs carreadoras de DOX. É demonstrado que partículas apresentando nanocorpos anti-EGFR promovem uma diminuição mais acentuada na viabilidade celular de células de câncer colorretal humano quando comparadas com partículas não decoradas. Concluindo, este trabalho apresenta a completa produção e caracterização de três nanoplataformas distintas e uma criteriosa avaliação *in vitro* de uma série de mecanismos celulares como endocitose, apoptose e autofagia. Os resultados alcançados sugerem que as construções aqui apresentadas possuem características que as colocam como nanoplataformas com aplicações clínicas em potencial, como plataformas de vacinas e sistemas de entrega de medicamentos.

Palavras chave: Nanotecnologia. Sistemas de entrega de medicamentos. Plataformas vacinais. Partículas proteicas. Partículas de ácidos nucleicos. Decoração de partículas. Doxorrubicina. Câncer.

SUMMARY

1. INTRODUCTION

The use of nanotechnology as a tool in the medical field is a global reality since the last century. In 1995, the U.S. Food and Drug Administration (FDA) authorized for the first time the commercial use of liposomes as carrier platforms for the chemotherapy drug doxorubicin (DOX) (Ventola, 2017). Since then, nanomedicine is considered an expanding market, with a number of 100 nanomedicines approved for commercialization and more than 650 formulations in clinical testing phases. Among them, it is possible to highlight constructions of different natures such as liposomes, polymers, viral vectors, protein-based and nucleic acids-based particles, among others (Shan *et al*., 2022).

Nucleic acid nanoparticles, also called NAMPs, has recently attracted the attention of researchers. Although their desirable characteristics such as programmability, 3D structure and biocompatibility, had already been known for some time, the demand for new technologies brought by COVID-19 pandemic led to an expansion in the study of NAMPs (Afonin *et al*., 2022). In fact, mRNA-based vaccines such as the Moderna and Pfixer/BioNTech area great example of formulations that were widely used during the COVID-19 pandemic (Jain *et al*., 2021).

Other remarkable class of nanoparticles is the protein-based ones, that can be obtained using simple methods, such as coacervation and emulsification of particles from a high-protein source, such as albumin solution; or by using modern methods, such as computational predictions and designing of new molecules (Hong *et al*., 2020; Galloway *et al*., 2021).

Despite their synthetic nature, the designing of many *de novo* proteins are inspired by living organisms. Artificial capsid proteins, for example, are based on enveloped virus structures – organisms that are able to produce self-assembly structures that protects their own genetic material. This class of proteins is largely used to develop virus-like particles (VLPs) (Heddle *et al*., 2017).

The use of artificial capsid proteins in nanoparticles production allows the construction of self-assembly platforms whose essential parameters, such as size, shape and surface composition, can be highly controlled. As an example, these platforms can be engineered to display specific epitopes in their surface, what can be used for medical purposes such as vaccines and drug-delivery systems (Heddle *et al*., 2017). In fact, around 72% of the nanoformulations under observation of FDA were developed to treat immunological disorders, infections or neoplasms (Shan *et al*., 2022).

Hence, this thesis aims the creation of inedited self-assembly nanoplatforms that use

double-strand nucleic acids as scaffold and artificial capsid proteins as nanocage as well as the *in vitro* evaluation of the physiological effects caused by these construction in tumoral and immune cell lines. Results are presented in three chapters.

In the first chapter is presented the creation and characterization of a new self-assembly DOX-carrier nanoparticle that uses DNA molecules as scaffold and is revested by the artificial capsid protein $C_4S_{10}K_{12}$. Moreover, it was evaluated the cell viability, cell uptake, apoptosis and autophagy mechanisms triggered in murine melanoma cells treated with free DOX or with DOX carried on this new platform. $C_4S_{10}K_{12}$ was kindly donate by Prof Renko de Vries' group, from the Wageningen University and Research – Netherlands. The experiments were performed at the Federal University of Viçosa, under supervision of Professor Anésia Santos. Data is presented in the original format of the paper "Virus-Like Particle-Encapsulated Doxorubicin Enters and Kills Murine Tumor Cells Differently from Free Doxorubicin", published in the journal Macromolecular Bioscience in April, 2023.

In the second chapter is presented the cloning, synthesis and purification of other inedited *virus-like* protein. Nevertheless, in addition to its self-assembly feature, this protein also allows the fusion of different epitopes in its surface via the Spy Catcher/Spy Tag system. The cloning, synthesis and purification of two peptides used in the decoration of the new developed protein is also presented. These proteins were used to revest DNA-based and double stranded RNA-based molecules. Finally, the cell uptake and immunogenicity of these particles were evaluated in two linages of antigen-presenting cells (APCs). These data were obtained during a PhD Sandwich period performed at the Wageningen University and Research, under the supervision of Professors Renko de Vries and Edwin Tijhaar. Data is presented in article format, to be submitted.

In the third chapter is presented the synthesis and purification of a new three-domain protein that bears a Spy Tag domain, a GFP domain and a domain called 7D12 – a nanobody that binds to the membrane protein EGFR (Epidermal Growth Factor Receptor), which is highly expressed in colorectal cancer cells. The new protein was coupled with the virus-like protein developed in Chapter 2 to produce DOX-carrying anti-EGFR decorated particles. The cytotoxic effect of the new construction upon colorectal cancer cells was evaluated as well as the comparation between nude particles and decorated particles effects on cell viability. The experiments described on Chapter 3 were performed at the Federal University of Viçosa, under the supervision of Professor Anésia Santos. Data is presented in article format, to be submitted.

REFERENCES

AFONIN, K. A. et al. Critical review of nucleic acid nanotechnology to identify gaps and inform a strategy for accelerated clinical translation. **Advanced Drug Delivery Reviews**, v. 181, p. e114081, 2022. DOI: https://doi.org/10.1016/j.addr.2021.114081.

GALLOWAY, J. M. et al. De Novo Designed Peptide and Protein Hairpins Self-Assemble into Sheets and Nanoparticles. **Small**, v. 17, n. 10, p. e2100472, 2021. DOI: https://doi.org/10.1002/smll.202100472.

HEDDLE, J. G.; CHAKRABORTI, S. and IWASAKI, K. Natural and artificial protein cages: design, structure and therapeutic applications. **Current Opinion in Structural Biology**, v. 43, p. 148-155, 2017. DOI; https://doi.org/10.1016/j.sbi.2017.03.007.

HONG, S. et al. Protein-Based Nanoparticles as Drug Delivery Systems. **Pharmaceutics**, v. 12, n. 7, p. e604, 2020. DOI: https://doi.org/10.3390/pharmaceutics12070604.

JAIN S. et al. Messenger RNA-based vaccines: Past, present, and future directions in the context of the COVID-19 pandemic. **Advanced Drug Delivery Reviews**, v. 179, p. e114000, 2021. DOI: https://doi.org/10.1016/j.addr.2021.114000.

SHAN, X. et al. Current approaches of nanomedicines in the market and various stage of clinical translation. **Acta Pharmaceutica Sinica B**, v. 181, p. e114083, 2022. DOI: https://doi.org/10.1016/j.addr.2021.114083.

VENTOLA, C. L. Progress in Nanomedicine: Approved and Investigational Nanodrugs. **P & T: a peer-reviewed journal for formulary management**, v. 42, n. 12, p. 742–755, dez. 2017. PMID: 29234213.

2. CHAPTER 1

VIRUS-LIKE PARTICLE-ENCAPSULATED DOXORUBICIN ENTERS AND KILLS MURINE TUMOR CELLS DIFFERENTLY FROM FREE DOXORUBICIN

RESEARCH ARTICLE

Macromolecular Bioscience
www.mbs-journal.de

Virus-Like Particle-Encapsulated Doxorubicin Enters and Kills Murine Tumor Cells Differently from Free Doxorubicin

Amanda P. Gonçalves, José Ésio B. Ramos, Karoline H. Madureira, Marcelo L. Martins, Anésia A. Santos, and Renko de Vries*

The use of nanoparticles as chemotherapeutic carriers has been suggested as a way to overcome a range of side effects associated with classical cancer treatment such as poor selectivity and tumor resurgence. Obtaining precise control of the size and shape of therapeutic nanoparticles is crucial to optimize the targeting of tumor sites. In this work, it is shown that a previously developed system of polypeptide encapsulating individual DNA molecules, that forms rod-shaped nanoparticles of precisely controlled aspect ratio, can be loaded with the DNA-intercalating chemotherapeutic drug doxorubicin (DOX). It is characterized the size and shape of the DOX loaded-Virus-Like DNA Particles (DOX-VLDP) and shown that in this system the DOX payload does not leak out. Through in vitro cell studies, it is shown that DOX-VLDP is internalized by melanoma tumor cells (B16F10 cells) in a delayed and endocytosis-dependent way culminating in increased cytotoxicity and selectivity to tumor cells in comparison with free DOX. In addition, it is found that DOX-VLDP trigger apoptosis and autophagy pathways in treated cells. Taken together, the data on the DOX-VLDP nanoparticles shows that they kill cancer cells differently from free DOX.

1. Introduction

The delivery of chemotherapeutic drugs to cancer cells in ways that minimize side-effects, has been the subject of intense research.[1,2] The administration of low molecular weight chemotherapeutics directly into the bloodstream is nonselective and this leads to many side effects and narrow windows of therapeutic efficiency, increasing the risk of tumor resurgence.[3,4] One strategy that has shown promise in improving the therapeutic index of classical chemotherapeutics is the use of nanoparticles as drug delivery systems (DDS). [1,2,5–7] In the cancer context, DDS leads to some degree of targeting where the chemotherapeutics are preferentially delivered to cancer cells, either through active targeting mechanisms such as receptor binding, or through passive targeting due to the enhanced permeability and retention (EPR) effect.[2,6,7]

Many researchers have explored the effects of nanoparticle size, shape, and surface chemistry on passive targeting mediated by EPR in solid tumors,[2,8] and while it is clear that nanoparticle geometry, size, and surface chemistry play an important role, there are no detailed rules yet for how to optimize the passive targeting of nanoparticles to cancer cells. Although there are some lipid formulations, including liposomes and micelles, approved by FDA as passive delivery agents for chemotherapeutic agents,[5] it has been shown convincingly that shape is a crucial parameter in determining passive targeting mechanisms.[5,8,9] For example, it was shown that the circulation time of rod-shaped micelles increases dramatically with micelle length, with important implications for passive targeting via EPR.[9]

In general, there are not so many well-defined high-aspect ratio nanoparticles that have been explored as delivery vehicles. However, our group has previously designed a sequence for a polypeptide that mimics certain viral capsid proteins that encapsulate nucleic acids (DNA or RNA) in rod-shaped Virus-Like Particles (VLPs).[10] For the case of double-stranded DNA (dsDNA) each VLP contains exactly one DNA molecule, with a length of ≈1/3 of the contour length of the DNA template, allowing the precise variation of the VLP length via the length of the DNA template.[10] This protein is abbreviated as C-S-B, whereC is a domain rich in glycine, proline, and other hydrophilic amino acids, S = $(GAGAGAGS)_{10}$ is a silk-like sequence that self-assembles into stiff ribbons via strong hydrogen-bond interactions and B = K_{12} nonspecifically binds to nucleic acids via strong electrostatic interactions.[10,11]

A. P. Gonçalves, A. A. Santos
Department of General Biology
Federal University of Viçosa
Viçosa, Minas Gerais 36570-900, Brazil
E-mail: amanda.patricia@ufv.br
J. É. B. Ramos, M. L. Martins
Department of Physics
Federal University of Viçosa
Viçosa, Minas Gerais 36570-900, Brazil
K. H. Madureira
Department of Genetics
Ecology and Evolution, Biological Sciences Institute, Federal University of Minas Gerais
Belo Horizonte, Minas Gerais 31270-901, Brazil
R. de Vries
Department of Physical Chemistry and Soft Matter
Agrotechnology & Food Sciences, Group, Wageningen University
Wageningen, Gelderland 6708 WE, The Netherlands

The ORCID identification number(s) for the author(s) of this article can be found under https://doi.org/10.1002/mabi.202200530

DOI: 10.1002/mabi.202200530

 © 2023 Wiley-VCH GmbH

Considering that many chemotherapeutics such as DOX are DNA intercalators,[12,13] that DNA can be used as a chelating polymer for the delivery of chemotherapeutics,[14–16] and the unique ability of C-S-B protein in forming rod-shaped nanoparticles of precisely controlled aspect ratio,[10] we here aimed to evaluate whether C-S-B DOX-loading DNA particles could be used as a passive targeting model of rod-shaped nanoparticles for cancer therapeutics. To achieve this, we here characterized DOX-VLDP and used in vitro cell studies to test their uptake and subsequent processing by B16F10 tumor cells.

2. Experimental Section

2.1. Materials

Template DNA used to assemble the VLPs were 2.5 Kbp DNA fragments (ThermoFisher, Vilnius, VNO, Lithuania). DOX Hydrochloride was from Sigma–Aldrich, St. Louis, MO, US. The C-S-B protein was produced and purified as described previously.[10]

2.2. DOX-VLDP Assembly

To assemble DOX-VLDP, 0.8 μL of DNA fragments [500 ng μL^{-1}] was mixed with 0.3 μL of DOX [7.3 mM] and 19 μL of Tris-HCl [10 mM] pH 7.4 buffer. The mixture was incubated in the dark at room temperature for 1 h to allow for DOX intercalation. Next, 5 μL of C-S-B protein [150 mg mL^{-1}] was added to the DNA-DOX mixture. This mixture was incubated at room temperature for 24 h to allow for complete coating of the DOX-loaded DNA by the C-S-B coating proteins. DOX-VLDP prepared in this way have a protein-to-DNA ratio ($r_{prot/bp}$) = 0.5, which represents 1 protein to each 2 base pairs (bp) of DNA; and a final concentration of DOX of 100 μM, which represents an excess of DOX molecules in relation to DNA bp. In this way, we guarantee the DOX-saturation of DNA template. After DOX-VLDP assembly, any remaining free DOX was removed by diafiltration using Microcon 10 K Centrifuge Filters (Merck Millipore, Cork, Ireland).

2.3. Atomic Force Microscopy Imaging of VLPs

The size and shape control of empty VLPs and DOX-loaded VLPs were determined using atomic force microscopy (AFM) imaging of dried samples of VLPs adsorbed on ultra-flat silicon wafers. DOX-VLDP were prepared with a final concentration of DNA bp of 15 μM, a $r_{prot/bp}$ of 0.5, and DOX to DNA bp ratios ($r_{dox/bp}$) of 0, 0.5, and 1. A volume of 20 μL of assembled VLPs was deposited on ultra-flat, plasma-cleaned silicon wafer substrates and incubated for 3 min to let the VLPs to adsorb. Next, coated substrates were gently rinsed with water and dried under a gentle stream of nitrogen gas. AFM imaging of samples was performed in air, using a Bruker-US Atomic Force Microscope in the ScanAsist mode.

2.4. Cell Culture

The B16F10 cells were donated by Dra. Mirian T. Paes Lopes (Department of Pharmacology, Federal University of Minas Gerais, UFMG, Minas Gerais, Brazil). The melan-a cell line (murine non-tumor melanocytes cells) was donated by Dr. Roger Chammas (Laboratory of Experimental Oncology, University of São Paulo, USP, São Paulo). B16F10 cells were cultured in DMEM medium (Sigma–Aldrich), melan-a cells were cultured in RPMI – 1640 medium, both at 37 °C, in a 5% CO_2 atmosphere. Both media were supplemented with 10% of fetal bovine serum (Gibco), 1% of penicillin (Sigma–Aldrich), 1% of streptomycin (Sigma–Aldrich), 0025% of amphotericin B (Sigma–Aldrich) and had their pH adjusted to 7.4.

2.5. FITC-Labeling of VLPs

Fluorescent labeling of VLPs was performed by mixing them with FITC (Sigma–Aldrich) solution. The isothiocyanate group of the fluorescent FITC reacts with the primary amines groups of the C-S-B protein. Final concentration of FITC in solution was 400 ng mL^{-1}. This mixture was incubated for 10 min in a dark tube and, after this time, free FITC molecules were removed by diafiltration using Microcon 10K Centrifuge Filters.

2.6. Characterization of DOX-VLDP Cell Uptake Using Fluorescence Microscopy

For visualizing DOX-VLDP, $\approx 5 \times 10^4$ cells were seeded in a35 mm glass plate (IBIDI) and then incubated with FITC-labeled DOX-VLDP [1 μM of DOX] for 1 h. After this, cells were imaged using an inverted LSM510 META laser scanning microscope (Zeiss) with an argon laser and a helium-neon laser with 40x objective at 490 nm (ex) and 525 nm (em). The pinhole was set to give a 1 to 1.5 μm optical slice. Post-acquisition image processing was done using Adobe Photoshop (Adobe Systems).

2.7. Fluorescence Microscopy Imaging of DOX Intracellular Release

Intracellular release of DOX from the VLPs was visualized using Fluorescence Microscopy (FM) of DOX fluorescence. Cells were seeded as described in Section 2.6 and treated with either DOX or with DOX-VLDP [1 μM] for, respectively, 3 and 12 h. After treatment, cells were observed using an inverted LSM510 META laser scanning microscope (Zeiss) with an argon laser and a helium-neon laser with 40x objective at wavelengths of 480 nm (ex) and 592 nm (em). The pinhole was set to give a 1 to 1.5 μm optical slice. Post-acquisition image processing was done using Adobe Photoshop.

2.8. Inhibition of Endocytic Pathways

For chemical inhibition of endocytic pathways, seeded cells (as-described in Section 2.6) were pretreated for by 1 h with a medium supplemented with Sucrose [0.4 M], Genistein [100 μg mL^{-1}] or Nystatin [50 μg mL^{-1}]. These chemicals are in- hibitors of, respectively, clathrin-dependent endocytosis, clathrin-independent endocytosis, and caveolin-dependent endocytosis. After the inhibitor treatment, cells were incubated with DOX

 © 2023 Wiley-VCH GmbH

or DOX-VLDP [1 μM] for 24, 96, and 168 h. Cells were visualized in a Biostation IMq Fluorescence Microscope (Nikon) at wavelengths of 545 nm (ex) and 620 nm (em). Intracellular fluorescence intensity was analyzed on ImageJ software by delimitation of individual cells and measurement of their Mean Grey Value. Approximately 30 individual cells were analyzed per condition.

2.9. Cytotoxicity Assay

Evaluation of cytotoxicity of DOX or DOX-VLDP for B16F10 cells was assayed using the MTT assay.[17,18] It was prepared one sample of DOX [100 μM] and one sample of DOX-VLDP [100 μM], as-described in Section 2.2, for each independent experiment. The treatment concentrations tested on cells (2.5 μM, 1.25 μM.0.625 μM and 0.313 μM) were obtained by serial dilution. In each well of a 96-well plate, 1×10^4 cells were suspended in 100 μL of medium. Cells were incubated at the conditions de- scribed in Section 2.4. After 24 h of incubation, the mediumof each well was replaced by 100 μL of medium + DOX, or medium + DOX-VLDP at the treatment concentrations. A con- trol group of cells was treated with medium only. In all cases, the time of incubation was 60 h. After incubation, the treatmentsolutions were replaced by 100 μL of 3-(4,5-Dimethylthiazol-2- yl)-2,5-Diphenyltetrazolium Bromide (MTT) [0.5 mg mL^{-1}] and cells were incubated for another 4 h. Next, the supernatantwas removed, the formazan crystals formed during MTT reac- tion were dissolved in 100 μL of dimethyl sulfoxide (DMSO) and the absorbance was measured at 570 nm using a Spec- traMax plate reader. MTT and DMSO were purchased fromSigma–Aldrich.

2.10. Detection of Apoptosis and Autophagy

To elucidate mechanisms of cell death and survival, Flow Cytometry (FC) and FM were performed for appropriately stained cells. For FC, cells were seeded at a density of 1×10^6 cells per well in a 6-well plate and treated with DOX or DOX-VLDP [1 μM]for 24 h. Next, cells were stained with Annexin V (Immuno- Tools) and Propidium Iodide (Sigma–Aldrich) and then analyzed using a BD FACSVerse Flow Cytometer. For FM, 1×10^4 cells were seeded in a 35 mm glass plate (IBIDI) and treated with DOX or DOX-VLDP [1 μM] for 24 h. After treatment, cells were stained with 100 μM of the autophagic vacuole-staining ligand monodansylcadaverine (MDC – Sigma–Aldrich) for 1 h and visualized in a Biostation IMq Fluorescence Microscope (Nikon) at wavelengths of 350 nm (ex) and 460 nm (em). Intracellular fluorescence intensity was analyzed on ImageJ software by delimitation of individual cells and measurement of their Mean Grey Value. Approximately 30 individual cells were analyzed per condition.

2.11. Data and Statistical Analysis of the Biological Experiments

Graphs and statistical analysis were performed using Graphpad Prism and R. Statistical tests are mentioned in the figures' captions, with $p < 0.05$ considered statistically significant for all analysis.

3. Results

3.1. Characterization of DOX-VLDP

Previously it was found[10] that a 2:1 molar ratio of protein to DNA [bp], after an incubation of 24 h, leads to a good coating of 2.5 Kbp DNA with C-S-B protein. The same DNA length and protein- to-DNA ratio are also used here for the VLPs that we addition- ally load with DOX. First, we compare the morphology of emptyVLPs with those prepared with DNA intercalated with DOX, at 1 DOX per bp. Representative Atomic Force Microscopy (AFM) images of empty and DOX-loaded VLPs are shown in **Figure 1**ab. Representative histograms of the contour length of the VLPs for both cases is given in Figure 1c,d. We find that DOX-VLDP has a rod-like shape, just like empty VLPs. Loading the VLPs with DOX notably increases the VLPs contour length (compare Figure 1a,b). As shown in Figure 1c,d, the peak of the contour length distribution shifts from ≈260 nm for empty VLPs (as reported previously[10]) to ≈400 nm for DOX-VLDP. The increase in length of the VLPs is not unexpected, given that DOX intercalation is known to increase the contour length of DNA[19,20] and since the contour length of the VLPs is proportional to the contour length of the DNA template.[10]

Since it is known that DOX fluorescence is strongly quenched when it is intercalated in DNA,[21,22] the saturation binding of DOX to DNA was calculated by fluorescence spectroscopy (Supporting Information, Figure SI-1a). We saw no significant fluorescence signal in $r_{dox/bp}$ lower than 0.25 – 0.3, what suggests that DNA molecule gets DOX-saturated when there is 1 DOX molecule for every 2.5–3 bp (Supporting Information, Figure SI-1b). Hence, the $r_{dox/bp} = 1$ used to load the VLPs represents a significant excess of DOX, that guarantees the saturation of the DNA template. We also observed a partial recovering of ≈15% on DOX fluorescence after addition of C-S-B protein to the system, what suggests that part of DOX is unbounded from DNA template during the self-assembly process (Supporting Information, Figure SI-1a).

After VLP assembly, they are diafiltrated to remove excess unbound DOX. Considering the excess of DOX used to saturate DNA template as well as the DOX released from DNA molecules after encapsulation, we assume therefore that the actual concentration of DOX that we deliver through the VLPs, is ≈70% lower than the concentration delivered with the DOX control.

3.2. In Vitro VLP Uptake and DOX Release by B16F10 Cells

For detecting VLPs inside cells using FM, the protein coating of the VLP is covalently labeled with FITC. DOX is fluorescent when not bound to DNA,[22] hence with FM we can directly monitor the release of DOX in cells. FM results of VLP uptake and DOX release for B16F10 cells are shown in **Figure 2**.

First, as shown in Figure 2b, FITC-labeled VLPs can be detected inside the B16F10 cells already after 1 hour of treatment, hence DOX-VLDP clearly successfully enter the cells. FITC-labeled VLPs were extensively washed (see materials and methods) hence fluorescence outside the cells is likely due to VLPs not internalized during the 1 h of incubation.

Next, we track release of DOX in the B16F10 cells, through the natural fluorescence of the DOX molecules. As shown in

 © 2023 Wiley-VCH GmbH

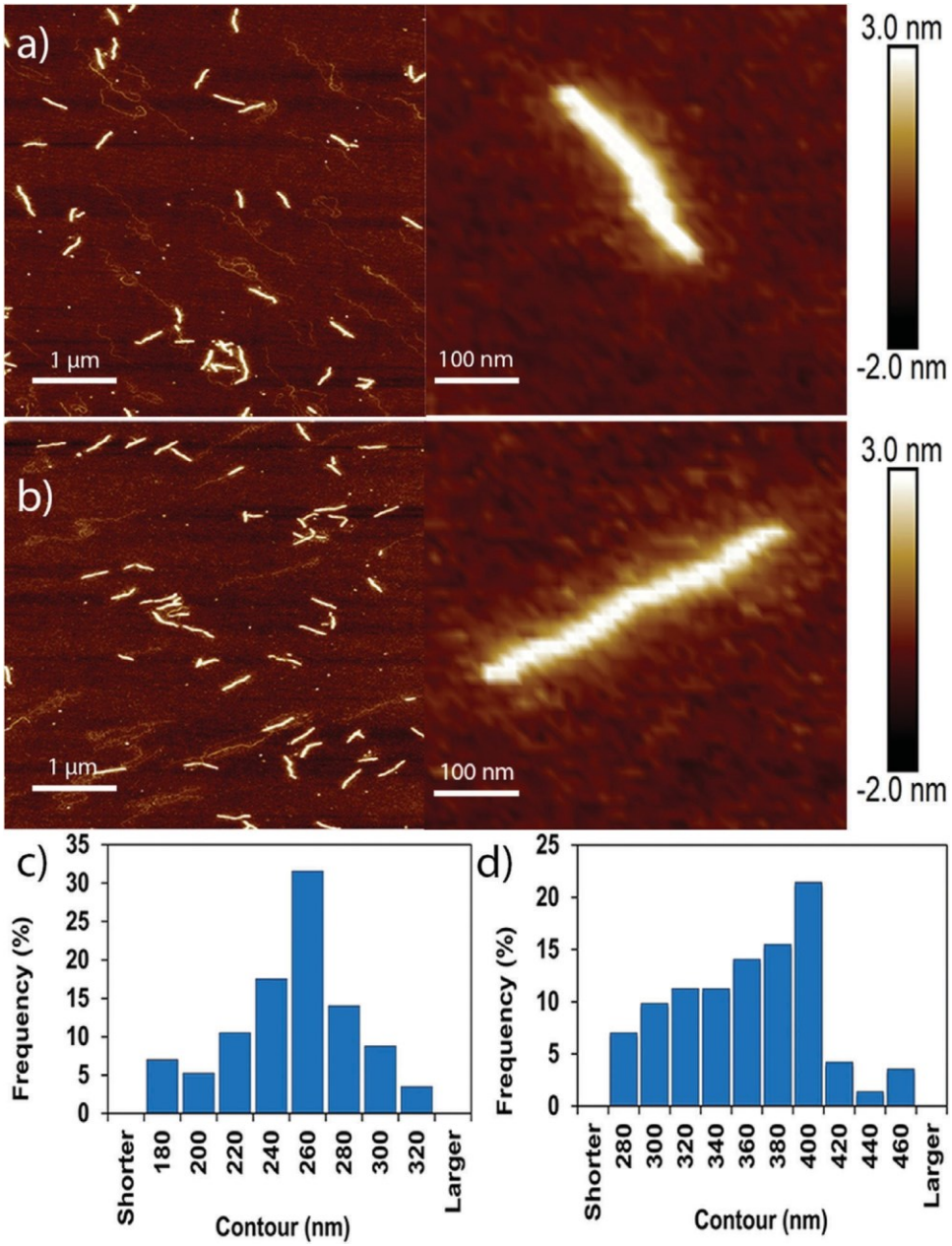

Figure 1. Characterization of DOX-VLDP using AFM imaging of dried complexes ($r_{dox/bp}$ = 0 in 1a and $r_{dox/bp}$ = 1 in 1b; $r_{prot/bp}$ = 0.5 in both cases). a) representative AFM image of empty VLPs; Right inset is a higher magnification of a single empty VLP. b) representative AFM image of DOX-VLDP; Right inset is a higher magnification of a single DOX-VLDP. c) Contour length histogram of empty VLPs obtained from AFM images. d) Contour length histogram of DOX-VLDP obtained from AFM images. For obtaining histograms, ≈70 particles were analyzed per condition.

Figure 2c,e, DOX can already be detected after 3 h (Figure 2c) and the signal persists until at least 12 h (Figure 2e). In contrast, for DOX-VLDP, there is no DOX signal at 3 h (Figure 2d), but it can be observed at 12 h (Figure 2f). In addition, after 24 h of treatment, we could still observe an overlapping of FITC and DOX fluorescence (Supporting Information, Figure SI-2), indicating that at this time part of DOX cargo and VLPs is colocalized and DOX-VLDP has not yet released their entire content into cells. This demonstrates that the VLPs properly release the DOX eventually, but this happens with a certain delay.

3.3. Characterization of Endocytic Uptake Pathway of DOX-VLDP

The delayed release of DOX for the case of DOX-VLDP sug- gests that the VLPs enter the cells through an active process, such as endocytosis. To establish whether this is the case, we investigated whether blockers of endocytic pathways influence the eventual release of DOX from the DOX-VLDP. Three dif- ferent blockers of endocytosis were added to cells prior to ex- posing B16F10 cells to either DOX or DOX-VLDP: Sucrose, a blocker of clathrin-dependent endocytosis; Genistein, a blocker

 © 2023 Wiley-VCH GmbH

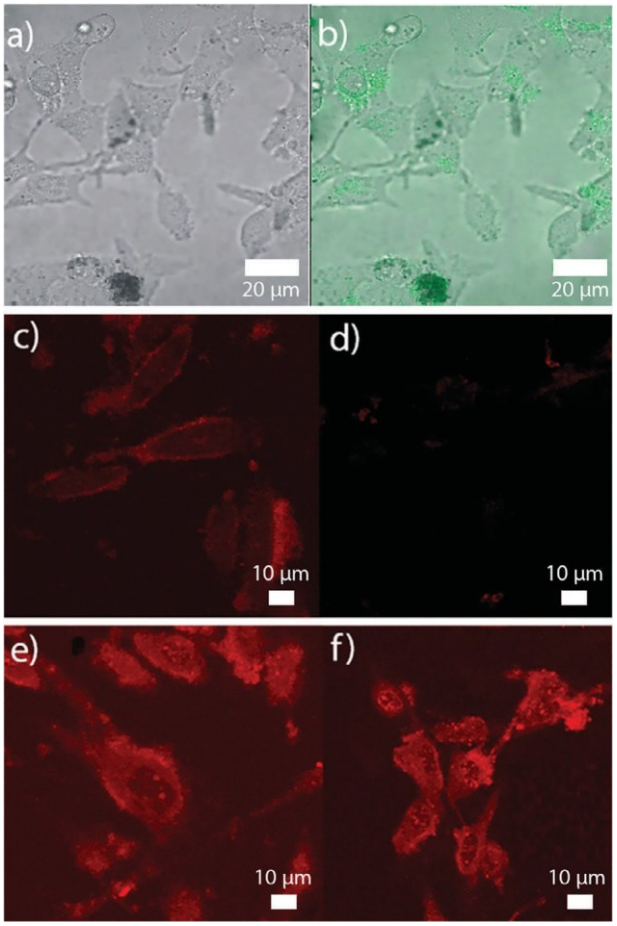

Figure 2. In vitro VLPs uptake and DOX release by melanoma cells. a) and b) B16F10 cells exposed for 1 h to FITC-labeled DOX-VLDP. a) bright field microscopy b) overlay of bright field microscopy with FM. Excitation at 490 nm, emission at 525 nm; 40x magnification. c)-f) FM of B16F10 cells exposed to DOX and DOX-VLDP, for respectively 3 and 12 h. Excitation at 480 nm, emission at 592 nm; 40x magnification. c) DOX, 3 h. d) DOX-VLDP, 3 h. e) DOX, 12 h. f) DOX- VLDP, 12 h.

of clathrin-independent endocytosis; and nystatin, a blocker of caveolin-dependent endocytosis.[23] Results of the blocking experiments are shown in **Figure 3**. We found that for incubation times of 24 h and 96 h there was a small effect of the various blockers (Supporting Information, Figures SI-3, and SI-4), but that the effect of the blockers was very clear for the longest incubation time of 168 h. For this longest incubation time, all blockers significantly reduced DOX release from the DOX-VLDP, but less so for the case of free DOX. This suggests that in the case of free DOX, the molecules enter cells by free diffusion through cellular membranes, as described by Speelmans and colleagues.[24,25] However, the DOX-VLDP require various endocytosis pathways to enter B16F10 tumor cells efficiently and to release their DOX payload.

3.4. Cytotoxicity and Cell Type Selectivity

Next, we analyzed cytotoxicity and cell type selectivity of DOX-VLDP as compared to free DOX. An MTT assay was employed to determine the cell viability. First the relevant controls were established: neither free DNA, nor free C-S-B protein, nor empty C-S-B/DNA VLPs reduce cell viability (Supporting Information, Figure SI-5). On the other hand, as shown in **Figure 4**, both DOX and DOX-VLDP reduce cell viability in a dose-dependent manner. Based on the concentration of DOX during loading of the VLPs, the reduction in cell viability is somewhat larger for DOX-VLDP, than for free DOX. It should be taken into account however, that the actual loading of the VLPs is significantly lower in view of the maximal number of DOX molecules that can be bound per DNA bp in the VLPs (r_{max}), which is ≈0.3, and the partial unbounding of DOX from template after protein encapsulation (r_{unb}), which is ≈0.15 (Supporting Information, Figure SI-1). Hence, we conclude that DOX-VLDP are significantly more toxic than free DOX for the B16F10 cells. We also evaluated toxicity of DOX and DOX-VLDP for nontumor melan-a cells and found only small difference between the dose dependence for these two cell lines (Supporting Information, Table SI-1).

3.5. Influence of DOX-VLDP on Apoptosis and Autophagy

Although we found small differences in cytotoxicity between B16F10 cells and non-tumor melan-a cells, this process may be triggered by different molecular mechanisms for both cases. For cancer cells, normally not only apoptosis but also autophagy is a tumor suppressor pathway, with the latter facilitating the degradation of oncogenic molecules.[26] However, under some conditions it has been found that autophagy can facilitate the survival of tumor cells and contribute to drug resistance.[27] Thus, we investigated the extent to which free DOX and DOX-VLDP activate apoptosis and autophagy pathways. We used annexin V-staining to quantify apoptosis by FC, and MDC-staining to detect autophagic vacuoles by FM. Results are shown in Figure 5.

As can be seen in Figure 5a,b, DOX-VLDP clearly trigger the apoptotic cell death pathway in B16F10 cells. Surprisingly however, as shown in Figure 5c--f, we also find that DOX-VLDP, but not free DOX, induce a significant increase of autophagic vacuoles for the B16F10 cells. This is not the case for the non-tumor melan-a cells, pointing to a clearly different molecular response of the non-tumor melan-a cells to DOX-VLDP, as compared to B16F10 tumor cells. Furthermore, B16F10 cells show a different molecular response to DOX-VLDP as compared to free DOX.

4. Discussion

An important reason for exploring nanoparticle delivery of DOX is the need to reduce side effects such as cardiopathy and mucositis.[28,29] To achieve this, it is crucial to understand how encapsulated DOX induces different effects in cells than free DOX, and also how the effect of encapsulated DOX is different for different cell types. Whereas DOX enters cells by passive diffusion, freely crossing the lipid cell membranes[24,25] we find that DOX loaded into VLPs, enters cells via endocytosis, as expected when encapsulated in a nanoparticle of significant size.[30–32] We also find there is a significant delay between DOX-VLDP uptake and the appearance of intracellular DOX fluorescence indicating the release of the DOX, possibly due to the time it takes lysosomes

 © 2023 Wiley-VCH GmbH

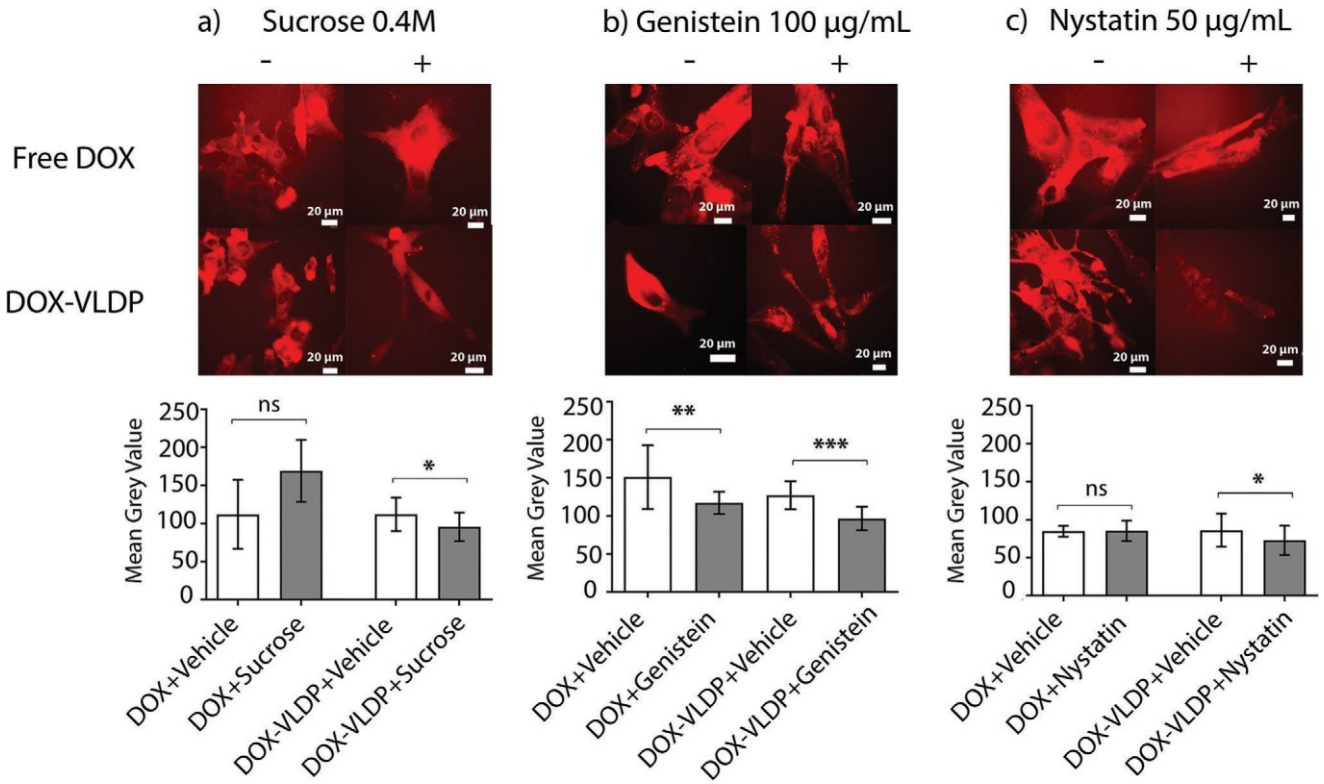

Figure 3. Effect of various blockers of endocytic pathways on DOX release. FM (excitation at 545 nm, emission at 620 nm; 20x magnification) of DOX release inside B16F10 cells as influenced by various blockers of endocytic pathways. Cells have been incubated for 168 h with either DOX or DOX-VLDP. Bars in lower row are the values of the average DOX Fluorescence. For obtaining data, ≈30 individual cells were analyzed per condition, from three independent experiments. Error bars are the standard deviation; asterisks represent a significant difference between treatments (p-value < 0.05; Student T-test). a) 0.4 M Sucrose. b) 100 µg mL^{-1} Genistein. c) 50 µg mL^{-1} Nystatin.

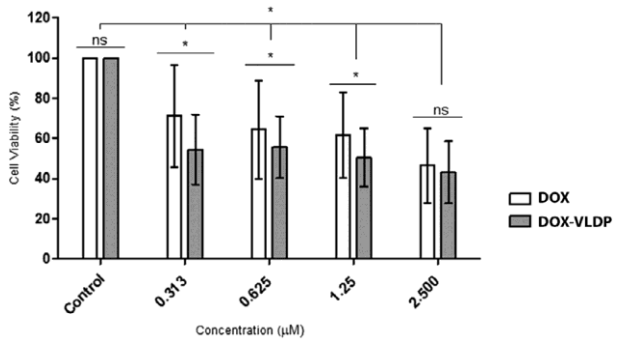

Figure 4. Cell viability was evaluated using MTT assay after 60 h of treatment of B16F10 cells with either DOX or DOX-VLDP. For the VLPs, the DOX concentration given is based on the concentration of DOX used during incubation with the template DNA, which likely is an overestimating, since $r_{max} \approx 0.3$ and $r_{unb} \approx 0.15$. Error bars are the standard deviation of four independent experiments. Asterisks represent a significant difference between treatments ($p < 0.05$; Chi-squared test for mixed model).

to degrade DOX-VLDP. Our results therefore indicate a significant impact of nanoparticle encapsulation on the processing of the DOX by the cells, as also found by others.[33–36]

Improving the selectivity of chemotherapy agents is one of the main goals in clinical and nanotechnology research applied to cancer.[37,38] Although we did not find a differential effect on cytotoxicity for the non-tumor melan-a cells and the B16F10 cells for DOX-VLDP, we showed that the cytotoxicity has different molecular characteristics for the two cell lines: whereas for the melan-a cells, it is mainly apoptosis that is induced, for the B16F10 cells it appears that additionally, the autophagy pathway gets activated by DOX-VLDP. In this case however, autophagy cannot be considered the main cell death mechanism, since DOX is widely known as an apoptotic promoter,[12] but an accessory mechanism in inducing cell death.

In fact, apoptosis and autophagy are not entirely uncoupled: several intermediate protein regulators are shared between these pathways.[39,40] It is thought that in tumor cells, autophagy plays a dual role that some researchers call "the autophagy paradox": in one hand, the recycling of the intracellular content supplies material to cells produce essential molecules, but on the other hand, digestion of intracellular contents can be interpreted as a signal to trigger apoptosis and other cell death pathways.[27,41] Our re- sult that DOX-VLDP appear to cell-selectively trigger autophagyfor the B16F10 cells but not for the melan-a cells, may possiblybe exploited in further work on achieving cell-type selective cytotoxicity of our construction.

5. Conclusion

In conclusion, here we show that our model of VLPs encapsulating DOX-loaded dsDNA forms controlled-size rod-shaped

 © 2023 Wiley-VCH GmbH

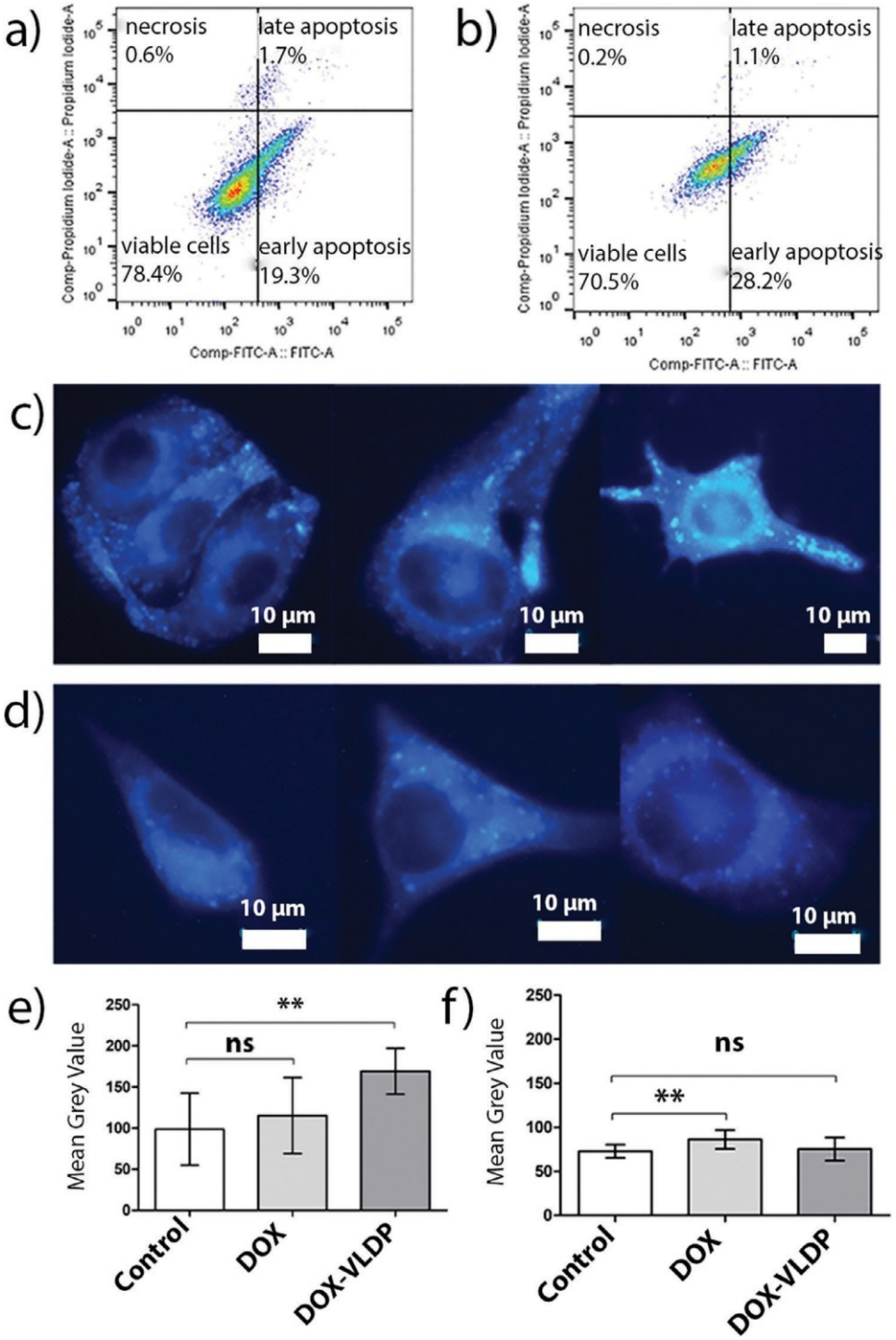

Figure 5. Influence of DOX-VLDP on apoptosis and autophagy. a) and b): flow cytometry with annexin V staining for the detection of apoptosis. a) control group (untreated B16F10 cells). b) treated group (B16F10 cells incubated for 24 h with DOX-VLDP). c – f) FM of B16F10 and melan-a cells pretreated with the fluorescent autophagy-marker MDC [100 µM] and subsequently treated with DOX or DOX-VLDP for 24 h. Excitation at 350 nm, emission at 460 nm; 80x magnification. c) representative micrographs for B16F10 cells. From left to right: untreated, treated with DOX, and treated with DOX-VLDP. d) representative micrographs for melan-a cells. From left to right: untreated, treated with DOX, and treated with DOX-VLDP. e) Bars representing the mean intracellular fluorescence intensity on B16F10 cells. f) Bars representing the mean intracellular fluorescence intensity on melan-a cells. For e) and f): For obtaining data, ≈30 individual cells were analyzed per condition, from three independent experiments. Error bars are the standard deviation; asterisks represent a significant difference between treatments (p-value < 0.05; One-way ANOVA, Dunnett's test).

 © 2023 Wiley-VCH GmbH

particles that do not let DOX cargo go until the VLPs are internalized by B16F10 cells in a delayed and endocytosis-dependent way. Furthermore, we find that the same concentration used to assembly DOX-VLDP is more toxic for B16F10 cells than free DOX and this cytotoxicity can be overestimated whether we consider that ≈70% of DOX used for preparing VLPs may not be used during self-assembling due to r_{max} and r_{unb} values.

In addition, we show that DOX- VLDP promotes cell death mediated by apoptosis, but autophagy pathway is also triggered. This happens in different ways in tumor or nontumor cells, suggesting a variation in the way different types of cells process DOX-VLDP and a possible route to increase the therapeutic index of DOX. We believe that these findings warrant further investigations of DOX-VLDP as a passive-targeting chemotherapeutic nanocarrier.

Supporting Information

Supporting Information is available from the Wiley Online Library or from the author.

Acknowledgements

The authors would like to acknowledge the Department of General Biology, the Department of Physics and the Nucleus of Microscopy and Microanalysis from the Federal University of Viçosa – Brazil, and the Physical Chemical Group from the Wageningen University and Research – The Netherlands, for providing the necessary experimental and technical support. This work was supported by the Brazilian agencies CAPES, CNPq, and FAPEMIG.

Conflict of Interest

The authors declare no conflict of interest.

Author Contributions

A.P.G., J.E.B.R, and K.H.M. conducted the experiments and analyzed the data. A.P.G wrote the manuscript. J.E.B.R., A.A.S., M.L.M., and R.V. validated the data, reviewed/edited the text, and provided/administered resources. All authors have read and agreed to the published version of the manuscript.

Data Availability Statement

The data that support the findings of this study are available from the corresponding author upon reasonable request.

Keywords

Doxorubicin, drug delivery systems, tumor cells, virus-like particles

Received: December 4, 2022
Revised: March 21, 2023
Published online:

[1] K. K. Jain, *Methods Mol. Biol.* **2020**, *2059*, 1.
[2] M. Sohail, W. Guo, Z. Li, H. Xu, F. Zhao, D. Chen, F. Fu, *Curr. Med. Chem.* **2021**, *28*, 3753.
[3] Y. H. Bae, K. Park, *J. Control Release* **2011**, *153*, 198.
[4] T. Sun, Y. U. S. Zhang, B. O. Pang, D. C. Hyun, M. Yang, Y. Xia, *Angew. Chem., Int. Ed.* **2014**, *153*, n/a.
[5] J. Shi, P. W. Kantoff, R. Wooster, O. C. Farokhzad, *Nat. Rev. Cancer* **2017**, *17*, 20.
[6] Y. Matsumura, H. Maeda, *Cancer Res.* **1986**, *46*, 6387.
[7] Y. Matsumura, *Jpn J. Clin. Oncol.* **2014**, *44*, 515.
[8] H. Maeda, W. Islam, *Polymer-Protein Conjugates From PEGylation and Beyond*, **2020**, Ch. 3, p. 41.
[9] Y. Geng, P. Dalhaimer, S. Cai, R. Tsai, M. Tewari, T. Minko, D. E. Discher, *Nat. Nanotechnol.* **2007**, *2*, 249.
[10] A. Hernandez-Garcia, D. J. Kraft, A. F. J. Janssen, P. H. H. Bomans, N. A. J. M. Sommerdijk, D. M. E. Thies-Weesie, M. E. Favretto, R. Brock, F. A. De Wolf, M. W. T. Werten, P. Van Der Schoot, M. C. Stuart, R. De Vries, *Nat. Nanotechnol.* **2014**, *9*, 698.
[11] M. W. T. Werten, W. H. Wisselink, T. J. Jansen-Van Den Bosch, E. C. De Bruin, F. A. De Wolf, *Protein Eng.* **2001**, *14*, 447.
[12] D. Gewirtz, *Biochem. Pharmacol.* **1999**, *57*, 727.
[13] G. Minotti, P. Menna, E. Salvatorelli, G. Cairo, L. Gianni, *Pharmacol. Rev.* **2004**, *56*, 185.
[14] Q. Jiang, C. Song, J. Nangreave, X. Liu, L. Lin, D. Qiu, Z. -. G. Wang, G. Zou, X. Liang, H. Yan, B. Ding, *J. Am. Chem. Soc.* **2012**, *134*, 13396.
[15] A. Samanta, I. L. Medintz, *Nanoscale* **2016**, *8*, 9037.
[16] L. He, J. Mu, O. Gang, X. Chen, *Adv. Sci.* **2021**, *8*, 2003775.
[17] T. Mosmann, *J. Immunol. Methods* **1983**, *65*, 55.
[18] P. Kumar, A. Nagarajan, P. D. Uchil, *Cold Spring Harb Protoc* **2018**, *2018*, 469.
[19] E. F. Silva, R. F. Bazoni, E. B. Ramos, M. S. Rocha, *Biopolymers* **2017**, *107*, e22998.
[20] C. Pérez-Arnaiz, N. Busto, J. M. Leal, B. García, *J. Phys. Chem. B* **2014**, *118*, 1288.
[21] P. Mohan, N. Rapoport, *Mol. Pharm.* **2010**, *7*, 1959.
[22] D. Agudelo, P. Bourassa, G. Bérubé, H. A. Tajmir-Riahi, *Int. J. Biol. Macromol.* **2014**, *66*, 144.
[23] M. Peng, N.a Yin, W. Zhang, *Cell Res.* **2010**, *20*, 223.
[24] G. Speelmans, R. W. H. M. Staffhorst, B. De Kruijff, F. A. De Wolf, *Biochem* **1994**, *33*, 13761.
[25] G. Speelmans, R. W. H. M. Staffhorst, H. G. Steenbergen, B. De Kruijff, *Biochim. Biophys. Acta* **1996**, *1284*, 240.
[26] M. Su, Y. Mei, S. Sinha, *J Oncol* **2013**, *2013*, 102735.
[27] C. Chen, L. U. Lu, S. Yan, H. Yi, H. Yao, D.i Wu, G. He, X. Tao, X. Deng, *Anticancer Drugs* **2018**, *29*, 1.
[28] P. K. Singal, N. Iliskovic, *N. Engl. J. Med.* **1998**, *339*, 900.
[29] C. M. Pinto, L. S. Horta, A. P. Soares, B. A. Carvalho, E. Ferreira, E. B. Lages, L. A. M. Ferreira, A. A. G. Faraco, H. C. Santiago, G. A. C. Goulart, *Pharmaceutics* **2021**, *13*, 1021.
[30] S. Zhang, J.u Li, G. Lykotrafitis, G. Bao, S. Suresh, *Adv. Mater.* **2009**, *21*, 419.
[31] A. Akinc, G. Battaglia, *Cold Spring Harb Perspect Biol.* **2013**, *5*, a016980.
[32] K. Debnath, S. Pal, N. R. Jana, *Acc. Chem. Res.* **2021**, *54*, 2916.
[33] G. V. Khutale, A. Casey, *Eur. J. Pharm. Biopharm.* **2017**, *119*, 372.
[34] U. Kanwal, N. Irfan Bukhari, M. Ovais, N. Abass, K. Hussain, A. Raza, *J. Drug Target* **2018**, *26*, 296.
[35] H. Tonbul, A. Sahin, E. Tavukcuoglu, G. Ultav, S. Akbas, Y. Aktas, G. Esendaglı, Y. Capan, *J. Drug Delivery Sci. Technol.* **2021**, *63*, 102535.
[36] S. Yang, M. K. Shim, W. J. Kim, J. Choi, G. I. H. Nam, J. Kim, J. Kim, Y. Moon, H. Y. Kim, J. Park, Y. Park, I. N. S. Kim, J. U. H. Ryu, K. Kim, *Biomaterials* **2021**, *272*, 120791.

© 2023 Wiley-VCH GmbH

[37] E. Biscop, A. Lin, W. V. Boxem, J. V. Loenhout, J. D. Backer, C. Deben, S. Dewilde, E. Smits, A. Bogaerts, *Cancers* **2019**, *11*, 1287.
[38] S. Akkın, G. Varan, E. Bilensoy, *Molecules* **2021**, *26*, 3382.
[39] S. W. G. Tait, G. Ichim, D. R. Green, *J. Cell Sci.* **2014**,*127*, 2135.
[40] S. Wanderoy, J. T. Hees, R. Klesse, F. Edlich, A. B. Harbauer, *Biol. Chem.* **2021**, *402*, 73.
[41] A. K. Verma, P. S. Bharti, S. Rafat, D. Bhatt, Y. Goyal, K. K. Pandey, S. Ranjan, S. A. Almatroodi, M. A. Alsahli, A. H. Rahmani, A. Almatroudi, K. Dev, *Oxid Med. Cell Longev* **2021**, *2021*, 88325.

 © 2023 Wiley-VCH GmbH

Macromolecular Bioscience

Supporting Information

for *Macromol. Biosci.*, DOI 10.1002/mabi.202200530

Virus-Like Particle-Encapsulated Doxorubicin Enters and Kills Murine Tumor Cells Differently from Free Doxorubicin

Amanda P. Gonçalves, José Ésio B. Ramos, Karoline H. Madureira, Marcelo L. Martins, Anésia A. Santos and Renko de Vries*

Virus-like particle-encapsulated doxorubicin enters and kills murine tumor cells differently from free doxorubicin

Amanda P. Gonçalves[1*], José Ésio B. Ramos[2], Karoline H. Madureira[3], Marcelo L. Martins[2], Anésia A. Santos[1] and Renko de Vries[4]

1 Department of General Biology, Federal University of Viçosa, Viçosa, 36570-900, Minas Gerais, Brazil
2 Department of Physics, Federal University of Viçosa, Viçosa, 36570-900, Minas Gerais, Brazil
3 Department of Genetics, Ecology and Evolution, Biological Sciences Institute, Federal University of Minas Gerais, Belo Horizonte, 31270-901, Minas Gerais, Brazil.
4 Department of Physical Chemistry and Soft Matter, Agrotechnology & Food Sciences Group, Wageningen University, Wageningen, 6708 WE, Gelderland, The Netherlands.

* Correspondence: amanda.patricia@ufv.br; Tel: +55-31-999296727. ORCID: https://orcid.org/0000-0002-5537-5104

Supplementary Methods

1. Fluorescence Spectroscopy

Fluorometric experiments were performed on a Agilent Technologies - Cary Eclipse Fluorescence Spectrophotometer. A sample of DOX solution at fixed concentration [2μM] was titrated with successive aliquots of DNA solution [200μM]. The excitation wavelength was set at 490 nm and the fluorescence emission spectra was collected in the range of 510 nm to 690 nm.

2. Fluorescence Microscopy imaging of cargo release from FITC-labeled VLPs

Intracellular release of DOX from the FITC-labeled VLPs was visualized using Fluorescence Microscopy (FM). Around 5×10^4 cells were seeded in a 35 mm glass plate (IBIDI®) and then

incubated with FITC-labeled DOX-VLDP [2.5 μM] for 24 hours. After treatment, cells were visualized in a Biostation IMq Fluorescence Microscope (Nikon®) at wavelengths of 490 nm (ex) and 520 nm (em), for FITC-labeled VLPs visualization; and of 555 nm (ex) and 590 nm (em), for DOX visualization.

3. Selectivity Index Estimation

DOX-VLDP cell selectivity was estimated by a Selectivity Index (SI) equation:

$$SI = \frac{nIC50}{tIC50}$$

Where, nIC50 is the concentration of compound that kills 50% of normal cells population and tIC50 the concentration of compound that kills 50% of tumor cells.

1. Supplementary Images

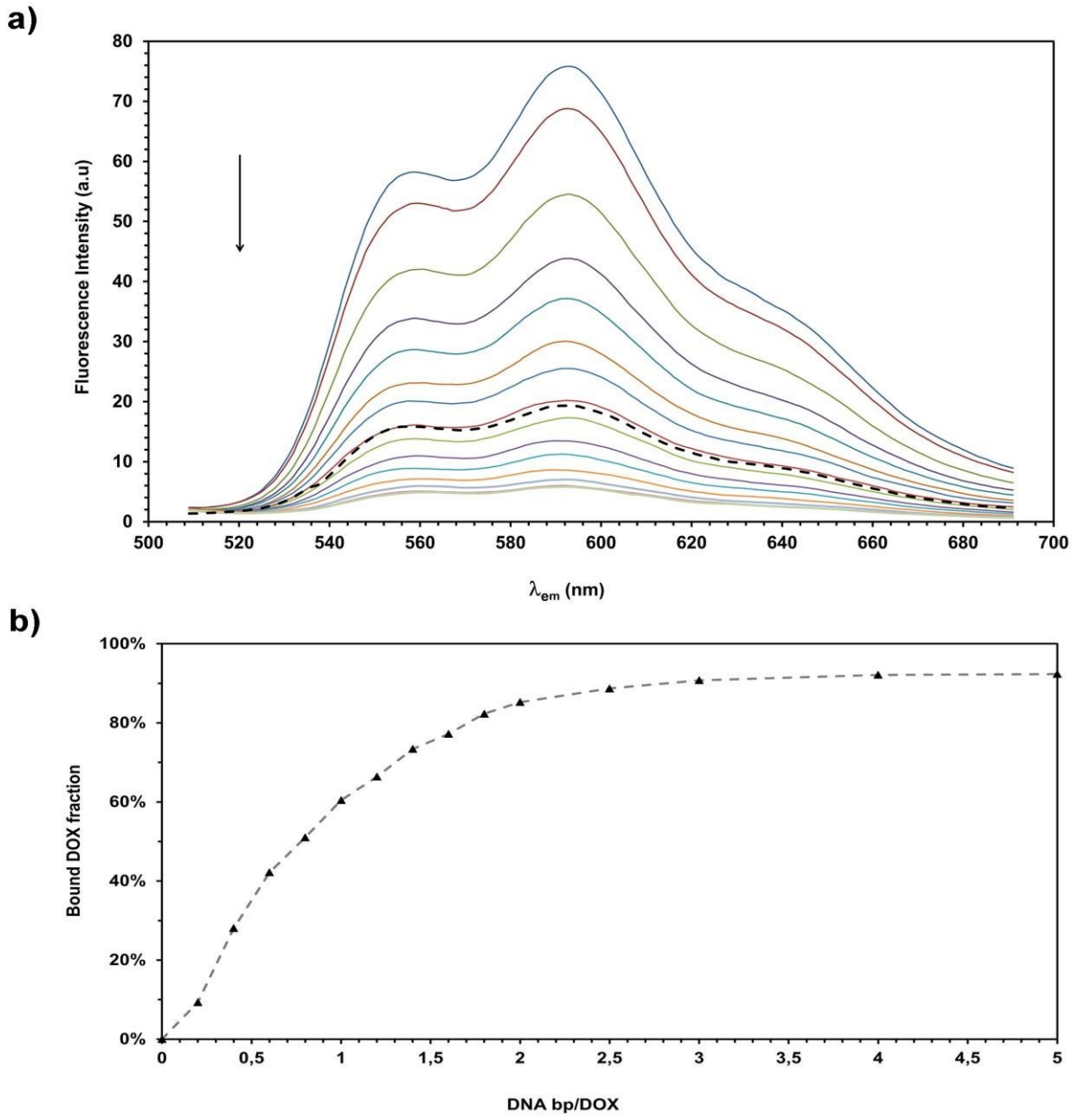

Figure SI-1. Fluorescence Spectroscopy of DOX bound to DNA molecules. a) Fluorescence Emission Spectra of DOX solution titrated with successive aliquots of DNA (excitation at 490 nm). The vertical arrow points in the direction of decreasing ratio ($r_{dox/bp}$); The dashed line shows the fluorescence spectrum of DOX/DNA complexes after addition of C-S-B protein at a ratio $r_{prot/bp} = 0.5$. b) Fraction of bound DOX estimated from fluorescence titration assay as a function of the ratio $1/r_{dox/bp}$, that is, the ratio of the number of DNA bp to the number of DOX molecules in solution. This curve in the figure is a guide to the eye.

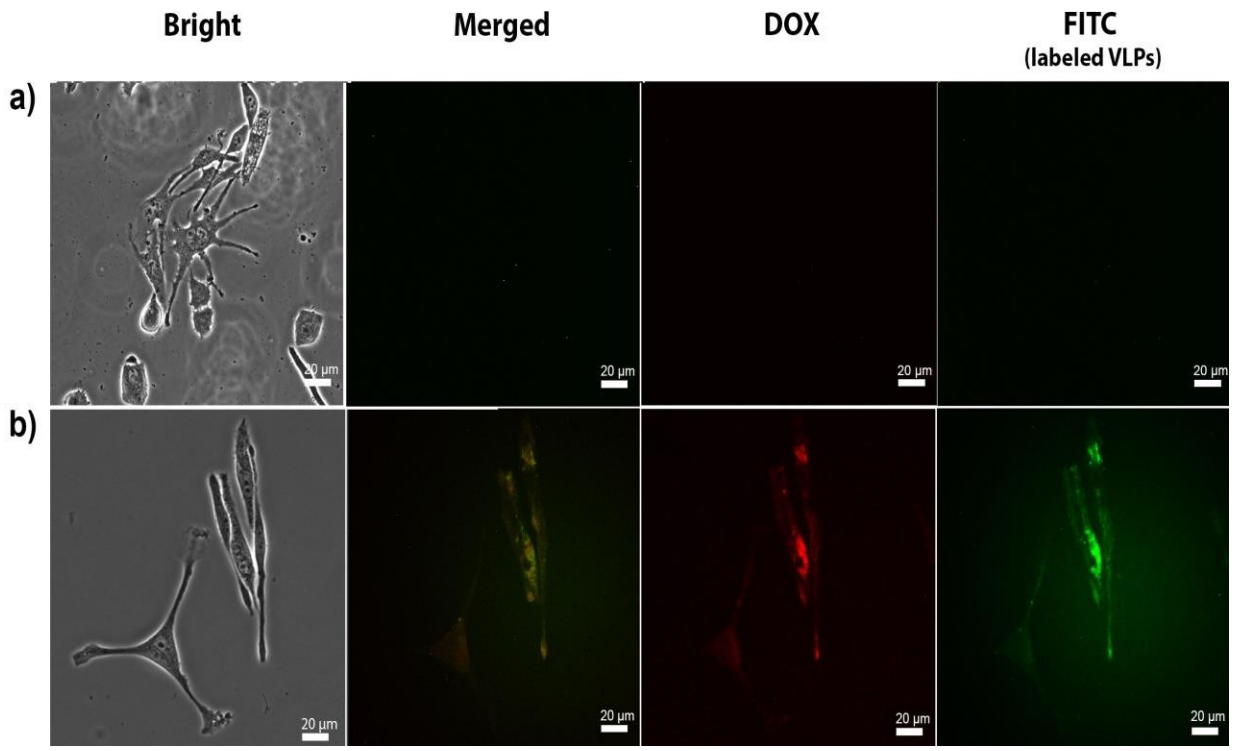

Figure SI-2: DOX-VLDP cargo release. Fluorescence microscopy showing colocalization of DOX cargo and FITC-labeled VLPs in B16F10 cells after: a) 0h of treatment. b) 24h of treatment. For obtaining FITC images: Excitation at 490 nm and emission at 520 nm; for DOX images: Excitation at 555nm and emission at 590 nm. 20x magnification.

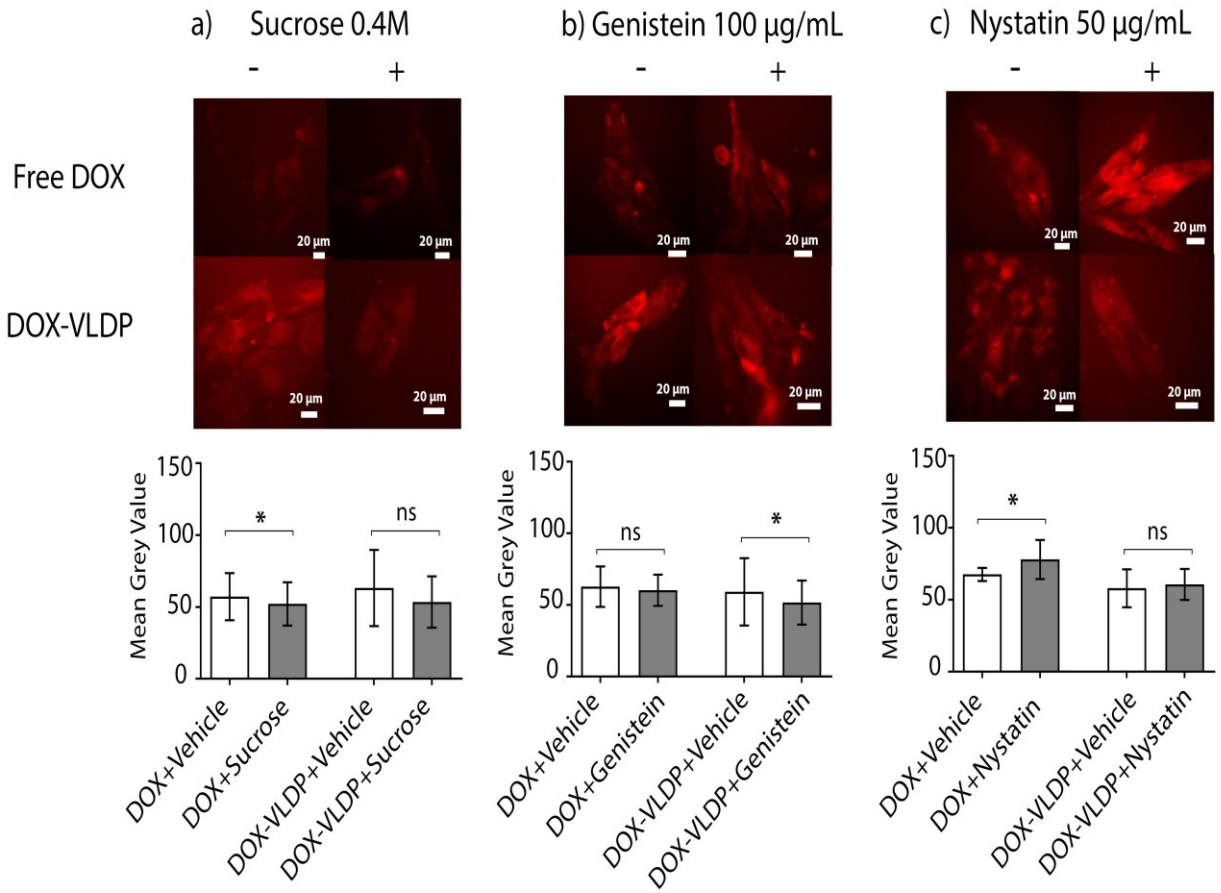

Figure SI-3. Effect of various blockers of endocytic pathways on DOX release. Fluorescence microscopy (excitation at 545 nm, emission at 620 nm; 20x magnification) of DOX release inside B16F10 melanoma cells as influenced by various blockers of endocytic pathways. Cells have been incubated for 24h with either DOX or DOX-VLDP. Bars in lower row are the values of the average DOX Fluorescence. For obtaining data, approximately 30 individual cells were analyzed per condition, from three independent experiments. Error bars are the standard deviation; asterisks represent a significant difference between treatments (p-value < 0.05; Student T-test). a) 0.4M Sucrose. b) 100 µg/mL Genistein. c) 50 µg/mL Nystatin.

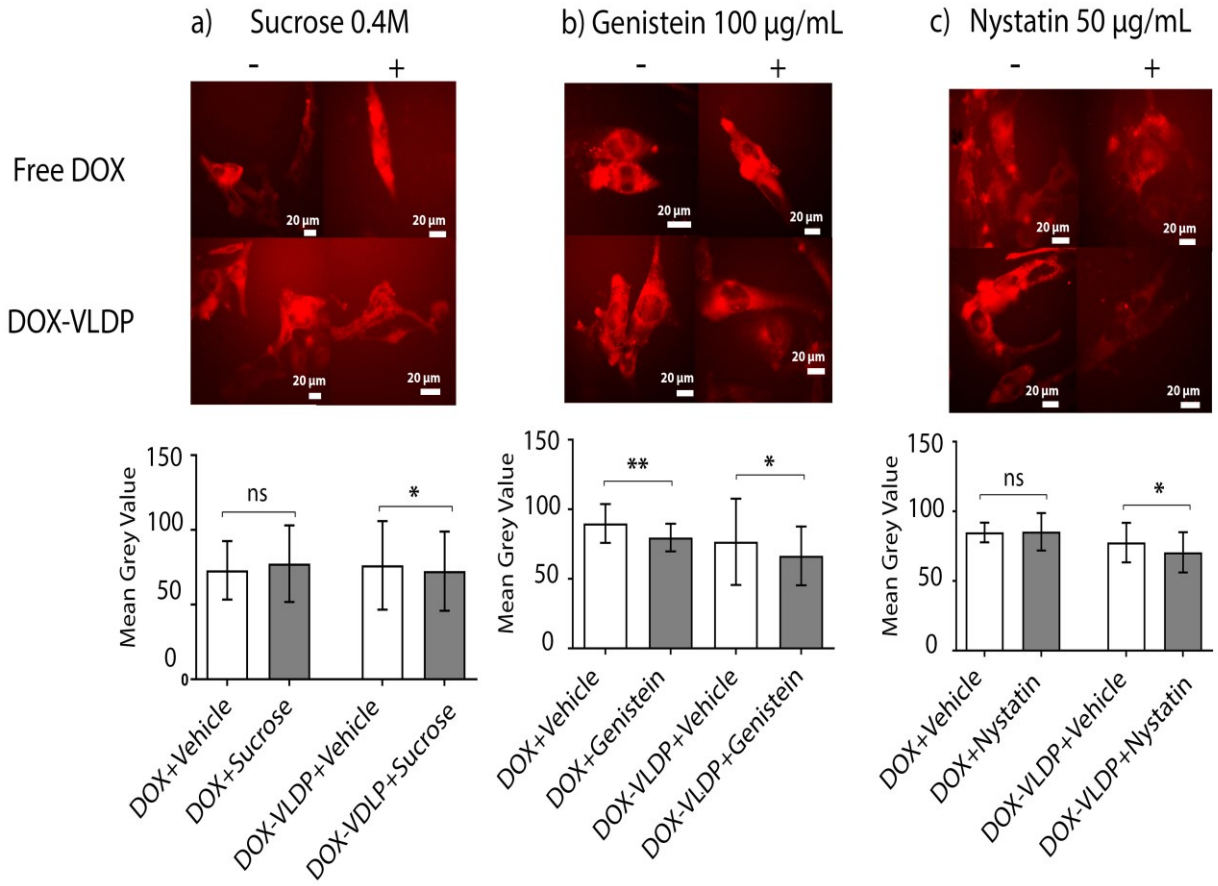

Figure SI-4. Effect of various blockers of endocytic pathways on DOX release. Fluorescence microscopy (excitation at 545 nm, emission at 620 nm; 20x magnification) of DOX release inside B16F10 melanoma cells as influenced by various blockers of endocytic pathways. Cells have been incubated for 96h with either DOX or DOX-VLDP. Bars in lower row are the values of the average DOX Fluorescence. For obtaining data, approximately 30 individual cells were analyzed per condition, from three independent experiments. Error bars are the standard deviation; asterisks represent a significant difference between treatments (p-value < 0.05; Student T-test). a) 0.4M Sucrose. b) 100 µg/mL Genistein. c) 50 µg/mL Nystatin.

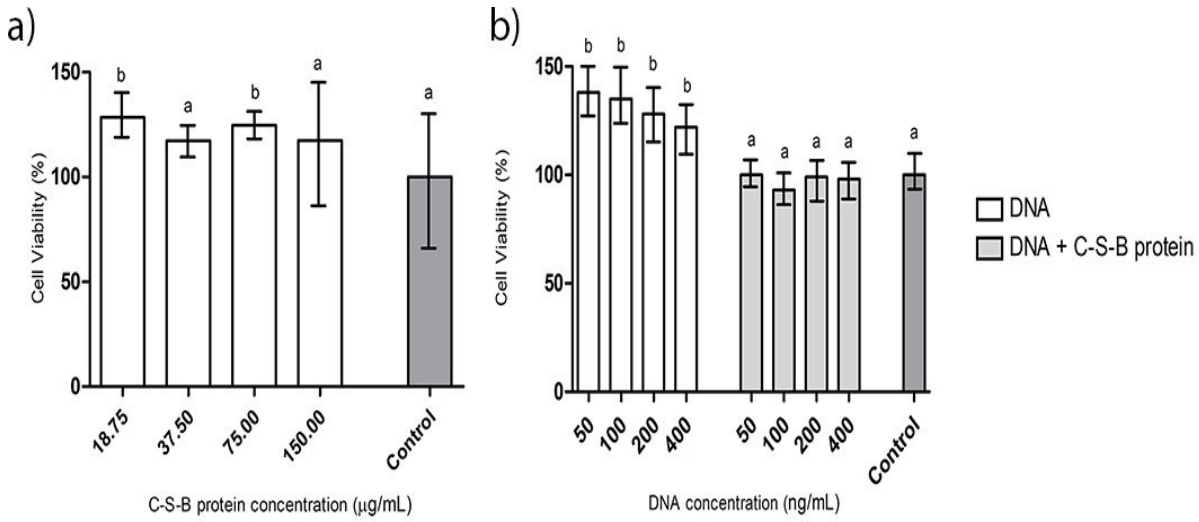

Figure SI-5. Cell viability evaluated using MTT assay after 60 hours of treatment of B16F10 cells. a) with C-S-B protein only. b) with non-coated and C-S-B-coated DNA molecules. Bars represent the standard deviation of five repetitions. Different letters represent statistical differences between treatments ($p < 0.05$; One-way ANOVA, Dunnett's test).

Table SI-1. Half Maximal Inhibitory Concentration values (IC_{50}) and Selectivity Index (SI) of DOX and DOX-VLDP.

Cell line	IC_{50} DOX (µM)	SI DOX	IC_{50} DOX-VLDP (µM)	SI DOX-VLDP
melan-a	0.929 ± 0.35	-	1.055 ± 0.42	-
B16F10	1.588 ± 0.39	0.59	0.971 ± 0.17	1.09

3. CHAPTER 2

PEPTIDE DISPLAYING ON SELF-ASSEMBLING NANOPARTICLES SURFACE PROMOTES CELL UPTAKE AND IMMUNE RESPONSES ON ANTIGEN-PRESENTING CELLS

Peptide Displaying on Self-Assembling Nanoparticles Surface Promotes Cell Uptake and Immune Responses on Antigen-Presenting Cells

Amanda P. Gonçalves [1], Rob de Haas[2], Anésia A. Santos[1], Edwin Tijhaar[3], Renko de Vries[2]

1 Department of General Biology, Universidade Federal de Viçosa, Viçosa, 36570-900, Minas Gerais, Brazil

2 Department of Physical Chemistry and Soft Matter, Agrotechnology & Food Sciences Group, Wageningen University, Wageningen, 6708 WE, Gelderland, The Netherlands

3 Department of Cell Biology and Immunology, Animal Sciences Group, Wageningen University, Wageningen, 6708 WD, Gelderland, The Netherlands

Abstract

Decorating virus-like particles (VLPs) with specific antigens has been largely used in the development of novel vaccine platforms. However, traditional methods of antigen conjugation to nanoparticles surface can offer a range of drawback such as platform unfolding and low binding of antigens. A current alternative to these methods is the Spy Catcher/Spy Tag system which is based in the ability of the peptides Spy Catcher and Spy Tag make strong and irreversible isopeptide bonds between them even when bigger structures are attached. Based on this, we developed a decorated VLPs incorporating the Spy Catcher/Spy Tag system to an unprecedent artificial capsid protein called NucleoX11. Our data shows that NucleoX11 is stable in both decorated and undecorated versions, forming self-assembly rod-shaped particles when incubated with double-stranded nucleic acids. Also, these decorated VLPs can be took up by antigen-presenting cells (APC) and enhance the expression of CD80 and CD86 molecules.

Keywords: Artificial Capsid Proteins, Decorated VLPs, Spy Catcher/Spy Tag, Vaccine Platforms.

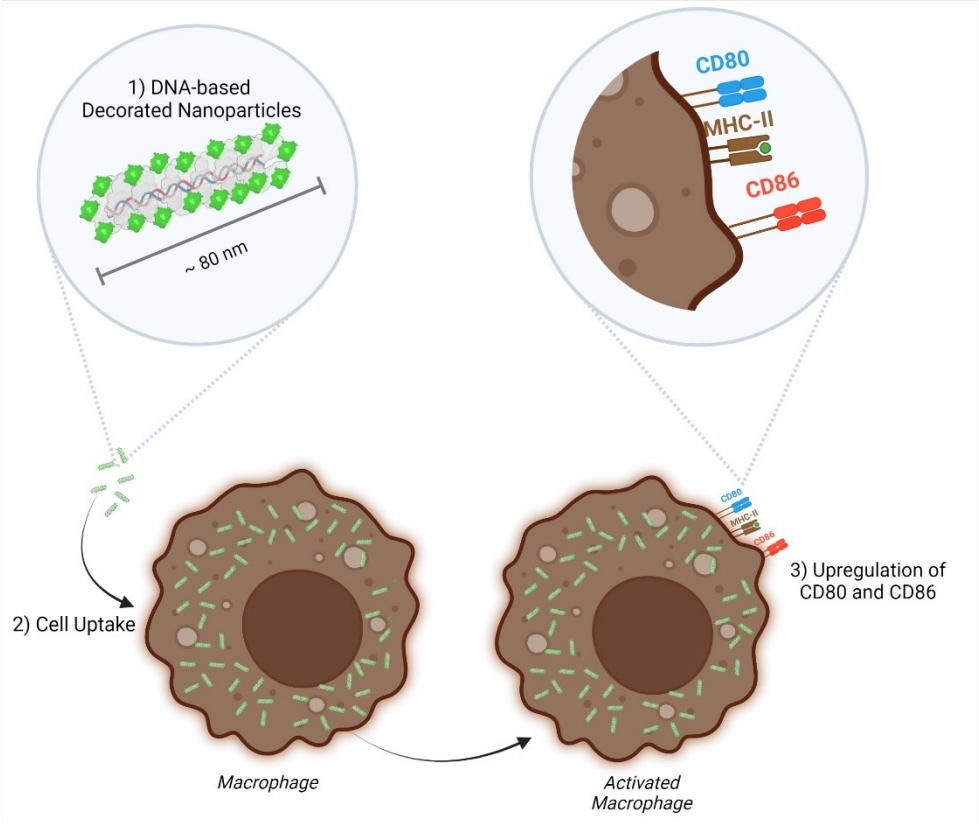

Figure 1 – Graphical Abstract.

1. Introduction

Nanotechnology has been commercially applied to medicinal purposes since 1989 being since then an important field on science and industry, receiving billion dollars of investment that increases year after year (Murphy *et al*., 1994; Zhang, 2019; Halwani, 2022). Among a variety of available nanoplatforms, the virus-like particles (VLPs) emerge as great candidates to clinical applications, especially in the immunology field, since this construction mimics natural organisms that can enter immune cells as well as triggers important physiological responses (Roldão *et al*., 2010).

Although VLPs can be directly obtained from natural organisms it is also possible to make this kind of construction in an artificial way, using nature as an inspiration to develop *de novo* capsid proteins (Heddle *et al*., 2017; Inaba and Matsuura, 2019). In this sense, a range of important features of VLPs produced for clinical application, such as size, shape, self-assembling control and biocompatibility can be finaly controlled (Heddle *et al*., 2017).

The ability of entering mammalian cells is another important feature that should be present in clinical VLPs. It is known that natural viruses can successfully enter and infect cells, mainly due to the specific bind of proteins displayed in their surface to receptor proteins located on cell host membrane (Maginnis, 2018).

In this sense, when designing a VLP it is necessary to think in elements that must be present in the construction that enhances its uptake by cells and tissues of interest. Displaying specific epitopes on VLPs surface can be a great strategy to achieve this goal (Al-Barwani *et al*., 2014; Zepeda-Cervantes *et al*., 2020). This can be done by either chemical or genetic fusion, however both methods can present some drawbacks, as VLPs modifications, misfolding and unbinding of displayed epitopes (Brune *et* al., 2016).

A current alternative to these traditional methods is the developing of artificial capsids proteins containing a Spy Catcher peptide domain (Veggiani *et al*., 2014). Spy Catcher is 138 amino acids peptide that forms a fast, strong and irreversible covalent bond with a smaller peptide containing 13 amino acids called Spy Tag (Zakeri *et al*., 2012). The Spy Catcher and Spy Tag peptides are well tolerated in both N-terminus and C-terminus of proteins without changing their conformation, making possible the design of a variety of scaffold proteins as well ligand peptides (Veggiani *et al*., 2014).

In fact, the expression of capsid proteins genetically fused with Spy Catcher has been used to produce a range of VLPs that can be decorated, displaying antigens in their surface. Considering the Spy Catcher/Spy Tag system stability as well as the variety of different antigens that can be displayed in a single Spy Catcher scaffold, these decorated VLPs have been strongly explored as potential vaccine platforms (Brune *et al*., 2016; Thrane *et al*., 2016; Wang *et al*., 2019; Heinimäki *et al*., 2022).

In this work, we developed and characterized decorated VLPs using the Spy Catcher/Spy Tag system. VLPs were developed by incorporating the Spy Catcher peptide in our *de novo* designed TALE-like protein NucleoX11, an artificial capsid protein that can forms rod-shape nanoparticles by self-assembling when incubated with double-stranded nucleic acids (de Haas *et al*. - Manuscript in preparation). We also developed the fluorescent attaching peptides SpyTag_sfGFP and SpyTag_sfGFP_OVA, making constructions that could be tracked in biological systems or carry immunogenic epitopes. With these materials, we aimed to investigate whether these constructions could be used with immunological purposes by

evaluating their cell uptake and stimulation of key immune markers on antigen-presenting cells (APC).

2. Material and Methods

2.1. Construction of expression vectors

SpyCatcher003_NucleoX11 construction was obtained by Golden Gate cloning. The sequence of interest was inserted in the plasmid PET24+ by using the BSaI-HFv2 digestion enzyme and the T4 ligation enzyme. After this, cloned plasmids were inserted on DH5α Competent *Escherichia coli* by bacterial cell transformation. Cloning efficiency was checked by DNA sequencing. Thus, cloned plasmids were inserted on expression cells (T7 Express Competent *E. coli*).

SpyTag003_sfGFP construction was obtained by inserting the commercial plasmid SpyTag003_sfGFP on DH5α *E. coli* by bacterial cell transformation. No cloning was needed. Plasmid quality was checked by DNA sequencing and then inserted on T7 *E. coli* expression cells.

SpyTag003_sfGFP_OVA construction was obtained by Restriction Enzyme cloning. The sequence of interest was inserted in the plasmid PET24+ by using the BamHI + XhoI digestion enzymes and the T4 ligation enzyme. After this, cloned plasmids were inserted on DH5α *E. coli* by bacterial cell transformation. Cloning efficiency was checked by DNA sequencing. Thus, cloned plasmids were inserted on T7 *E. coli* expression cells.

2.2. Protein purification

SpyCatcher003_NucleoX11 recombinant protein was obtained by IMAC protein purification using nickel columns in a HPLC. Purity was checked by denaturing SDS page and contaminants were removed by dialysis in a 20kDa MWCO membrane. Final product was stored at –20°C diluted in PBS pH 7.4 + 10% glycerol.

SpyTag003_sfGFP and SpyTag003_sfGFP_OVA recombinant protein was also obtained by IMAC protein purification, but using nickel charged resin in gravity columns. Purity was checked by denaturing SDS page and contaminants were removed by Size

Exclusion Chromatography in a Superdex® 200 10/300 GL column. Final product was stored at –20°C diluted in PBS pH 7.4 + 10% glycerol.

2.3. SpyCatcher_SpyTag protein coupling

Proteins containing the Spy Catcher and Spy Tag peptides were incubated together for 1.5 hours at 25°C in different Spy Tag/Spy Catcher (TC) ratios. Coupling efficiency was checked by denaturing SDS page.

2.4. Protein-Covering calculation

Here, we considered the amount of protein (in μM) necessary to cover 100% of a nucleic acid molecule as the protein cover (PC) ratio = 1.

Considering that one single NucleoX11 molecule cover approximately 11bp of double-stranded nucleic acids, the amount of protein (in μM) necessary to give PC ratio = 1 was calculated based on the following equation:

*PC ratio 1 (μM) = Nucleic acid concentration (μM) * [1/11 * nucleic acid fragments size (bp)]*

2.5. Self-assembly of Decorated Nanoparticles

Coupled SpyCatcher_SpyTag products in different TC ratios were incubated with dsDNA 250 bp fragments (Thermo Fisher®) at the concentration of 15 ng/μL for at least 1h at room temperature in a protein covering (PC) ratio = 3. DNA-protein complexes binding was checked by Electrophoretic Mobility Shift Assay (EMSA) in 1% agarose gel (45 min/100v) using 1X TAE buffer.

2.6. Atomic Force Microscopy (AFM)

AFM samples were prepared by adding 10 μL of DNA-protein complexes ([DNA] = 1 ng/μL; PC ratio = 1; TC ratio = 0 or 0.5) onto a clean silicon wafer. After 1 min, the wafer was washed with 1 mL of MQ water to remove salts and unbonded complexes. Liquid excess was carefully soaked with paper tissues and wafer was dried under slow N_2 stream. DNA-protein

complexes were visualized in a Bruker-US AFM machine in the Scan Asyst imaging mode. Image processing was performed with NanoScope Analysis software; First-order flattening was used for all images.

2.7. Cell culture

RAW cell line was established from murine macrophages and DC 2.4 cells from murine dendritic cells, all provided by the Department of Cell Biology and Immunology, Wageningen University and Research, The Netherlands.

Cells were cultured 75 cm² plastic flasks containing RPMI 1640 GlutaMAX™ medium supplemented with 10% Fetal Bovine Serum, 100 µg/mL antibiotics (Streptomicin and Penicillin) and 2 mM L-Glutamin at controlled temperature (37°C) and atmosphere (5% CO_2, 95% relative humidity).

2.8. Sample preparation of DNA-Protein particles for cell experiments

Nanoparticles were prepared by incubating coupled SpyCatcher_SpyTag products with dsDNA 250 bp fragments or a mix of fragments of dsRNA poly I:C (InvivoGen®) at a concentration of 15 ng/µL in a TC ratio = 1.5 and PC ratio = 1. Soluble SpyTag control was prepared by incubating SpyTag protein only. Incubation was performed overnight at 4°C. Inactivation of possible endotoxins on samples was ensured by adding polymyxin B to the samples at a final concentration of 50 µg/mL.

2.9. Cell uptake evaluation

Evaluation of particles cell uptake in RAW cells and DC 2.4 cells was performed by Fluorescence-Activated Cell Sorting (FACS). Around $3x10^5$/well of cells were seed in a 24-well plate and let to recovering for 2 hours at 37 °C and 5% CO_2 atmosphere. After this, plate medium was replaced by medium + nanoparticles in the desired concentrations and then, cells were incubated for 24 hours at 37 °C and 5% CO_2 atmosphere. In the next day, cells were prepared to FACS performing. Each well of the 24-well plate was washed with 800 µL of cold PBS 1x pH 7.4 and then cells were detached from plate surface, resuspended in 300 µL of cold FACS buffer ([BSA] = 1% in PBS 1x pH 7.4) and transferred to a 96-well NUNC plate. FACS

measurement was performed in a CytoFLEX LX Flow Cytometer. Median Fluorescence Intensity (MFI) of GFP-positive cells was extracted in the FITC channel.

2.10. CD80 and CD86 expression evaluation

Evaluation of internalized particles-mediated expression of the ligands CD80 and CD86 in RAW cells was also performed by FACS. Cells were prepared as described in the previous section, but the FACS buffer was supplemented with two monoclonal antibodies (mAb): BV421 anti-mouse CD80 and PE anti-rat CD86 [mAb dilution = 1:75]. MFI of CD80-positive cells was extracted in the PB channel and CD86-positive cells was extracted in the PE channel.

2.11. Statistical Analyses

Statistical analyses were performed using the software GraphPad Prism. Cell Uptake and Expression of CD80 and CD86 experiments were expressed as the average and standard deviation of MFI of GFP-positive cells or PB/PE-positive cells. Groups were compared with One-way ANOVA and Tukey's test posttest. Each test was considered statistically significant when the P value < 0.05.

3. Results and Discussion

3.1. Characterization of a novel DNA-Based Nanoparticle

The NucleoX11 is a *de novo* designed tale-like protein that binds to phosphate groups of nucleic acids, forming rod-shaped nanoparticles by self-assembling (de Haas *et al*. - Manuscript in preparation).

The insertion of the peptide SpyCatcher003 on N-terminus of NucleoX11 generated the SpyCatcher003_NucleoX11 construction, whose molecular weight estimation is 54.3 KDa (See Supplementary Data)[1].

[1] Supplementary data will not be presented in this thesis since they display nucleotide and amino acid sequences that will be part of another publication that must be submitted before this one, whose first authorship will be given to the co-author Rob de Haas.

SpyCatcher003_NucleoX11 was successfully obtained by IMAC protein purification, achieving a product of approximately 50 KDa, what is consistent with our *in-silico* predictions (Fig. 2).

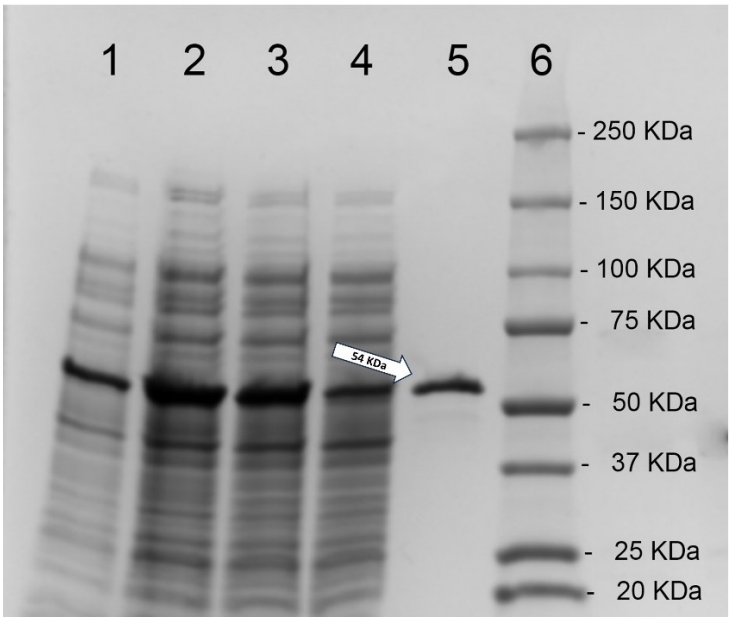

Figure 2 – SDS Page performed with SpyCatcher003_NucleoX11 protein purification product. A strong band with not much more than 50 KDa can be visualized (white arrow). 1) *E. coli* extract after IPTG induction; 2) Protein lysate; 3) *E. coli* supernatant; 4) IMAC column flow-through; 5) IMAC column elution; 6) Protein Marker.

It is important to note that the successfully insertion of the SpyCatcher003 peptide on NucleoX11 sequence did not impact the functionality of the protein. Data from EMSA essays shows that 250 bp DNA fragments had their mobility reduced when incubated with the SpyCatcher003_NucleoX11 protein, what suggest the formation of DNA-Protein particles (Fig 3A). In fact, these particles could be visualized by AFM and, as expected, they display a rod shape with approximately 80 nm of length, what is consistent with the 250 bp DNA fragments size (Fig 3B). Thus, we developed a stable and versatile nanoplatform that can display on its surface a variety of epitopes as long as these are conjugated to a SpyTag003 peptide.

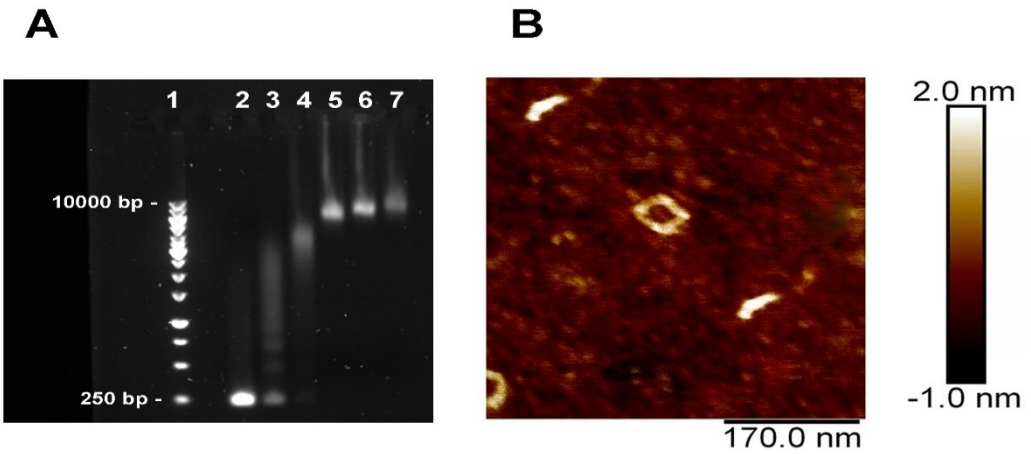

Figure 3 – Stability Assays with undecorated nanoparticles. **A)** EMSA performed with particles of 250 bp dsDNA + SpyCatcher_NucleoX11 protein in different PC Ratios: 1) DNA Ruler; 2) PC ratio = 0 (DNA only); 3) PC ratio = 0.25; 4) PC ratio = 0.5; 5) PC ratio = 1; 6) PC ratio = 1.5; 7) PC ratio = 3. **B)** Visualization of particles at PC Ratio = 3 by AFM.

3.2. Characterization of SpyTag decorating variants

Two SpyTag003 variants were also developed: one conjugated with the sfGFP protein and another conjugated with the sfGFP protein and specific aminoacidic fragments from Ovalbumin protein, here called OVA (See Supplementary Data).

Both SpyTag003_sfGFP and SpyTag003_sfGFP_OVA were successfully obtained by IMAC protein purification, achieving products consistent with the *in-silico* predictions, with 30.4 KDa and 41.4 KDa, respectively (Fig. 4).

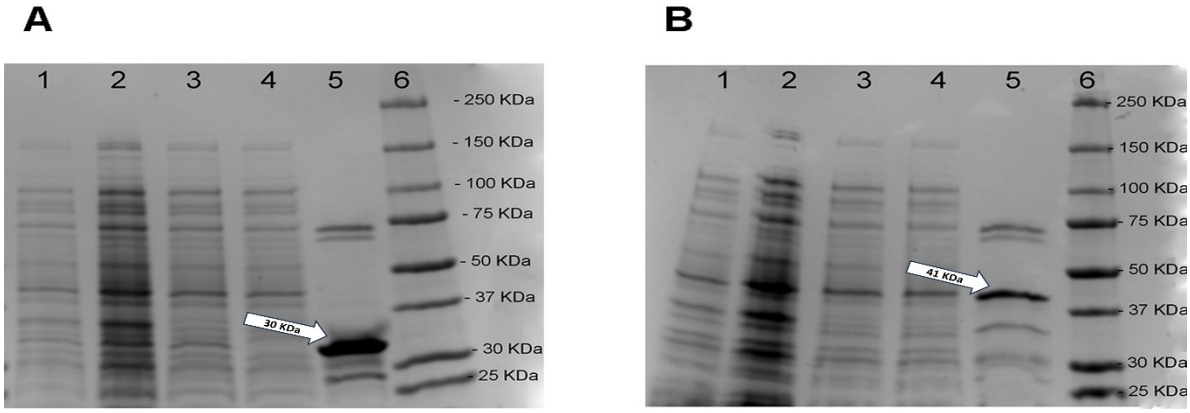

Figure 4 – SDS Page. **A)** Performed with SpyTag003_sfGFP protein purification product. A strong band with around 30 KDa can be visualized (white arrow). **B)** Performed with SpyTag003_sfGFP_OVA protein purification product. A strong band with around 40 KDa can be visualized (white arrow). In both figures, numbers represent: 1) *E. coli* extract after IPTG induction; 2) Protein lysate; 3) *E. coli* supernatant; 4) IMAC column flow-through; 5) IMAC column elution; 6) Protein Marker.

To have different Spy Tag products allowed the achieving of two distinct nanoparticles, each one displaying different compounds but having the same scaffold.

The sfGFP decorating was chosen due its tracking purpose, especially on cell models, once the fluorescent particles can be visualized and/or detected by fluorescence microscopy, flow cytometry and plenty of methodology.

On the other side, the sfGFP_OVA decorating was chosen due the intrinsic immunogenicity of OVA fragment, what contains two small aminoacidic sequences that can trigger both bind to MHC-1 and MHC-2 complexes, triggering peptide presentation processes (Johnsen and Elsayed, 1990; Dersh *et al*., 2019). The maintaining of the sfGFP was chosen to keep the tracking feature. Therefore, sfGFP_OVA decorating could be tracked in cell models and also indicate whether the particles produced with the SpyCather003_NucleoX11 protein could be used for antigen presentation purposes, as vaccine platforms for example.

3.3. Assembly of Decorated Nanoparticles

Coupling of SpyCatcher003_NucleoX11 and SpyTag003 protein variants was effective in all TC Ratios tested (Fig. 5). It is possible to see that whereas the Spy Tag concentration increases, a stronger band appears around 100 KDa, suggesting that that the two proteins are bounded in a covalent way and, besides this effect does not depend of Spy Tag concentration, this concentration is determinant to generate proteins more or less coupled.

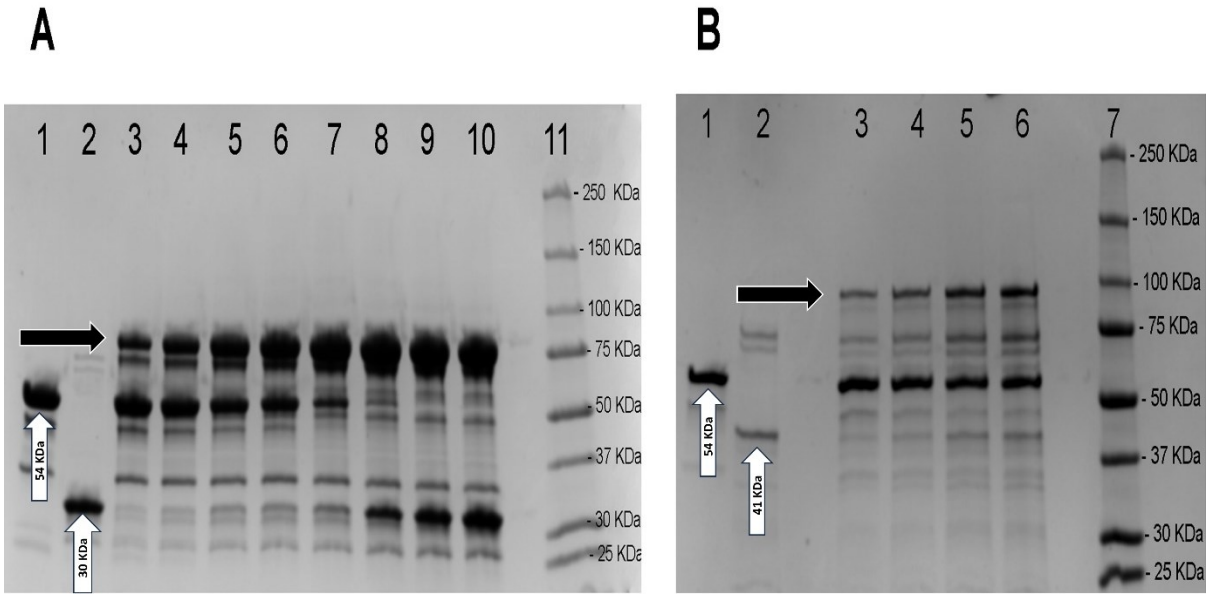

Figure 5 – Coupling Assay. SDS Page. A new product with a higher molecular weight is formed when we mix 1 and 2 in different ratios (black arrow) **A)** SDS Page performed with SpyCatcher003_NucleoX11 conjugated with

SpyTag003_sfGFP in different TC Ratios: 1) SpyCatcher control; 2) SpyTag control; 3) TC ratio = 0.5; 4) TC ratio = 0.75; 5) TC ratio = 1; 6) TC ratio = 1.25; 7) TC ratio = 1.5; 8) TC ratio = 2; 9) TC ratio = 2.5; 10) TC ratio = 3; 11) Protein marker. **B)** SDS Page performed with SpyCatcher003_NucleoX11 conjugated with SpyTag003_sfGFP_OVA in different TC Ratios: 1) SpyCatcher control; 2) SpyTag control; 3) TC ratio = 0.5; 4) TC ratio = 1; 5) TC ratio = 1.5; 6) TC ratio = 2; 7) Protein marker.

Figure 5A shows that from the 1.5 TC ratio the bands around 30 KDa, representing the SpyTag003_sfGFP proteins, became stronger again. This suggests that the saturating TC ratio is 1.5 and after this no more coupling is allowed. On this way, for SpyCatcher003_NucleoX11 and SpyTag003_sfGFP_OVA proteins the coupling effect was tested with a maximum TC ratio of 2 (Fig. 5B).

The coupled proteins were incubated with dsDNA to promote the self-assembling of particles. The SpyCather/SpyTag coupling did not impaired the formation of DNA-protein particles, that produced rod-shaped particles just like before the SpyTag attaching (Fig 6). On this way, we demonstrated that the particles produced with the SpyCatcher003_NucleoX11 does not lose their functionality, stability and shape when they are decorated with SpyTag003 variants.

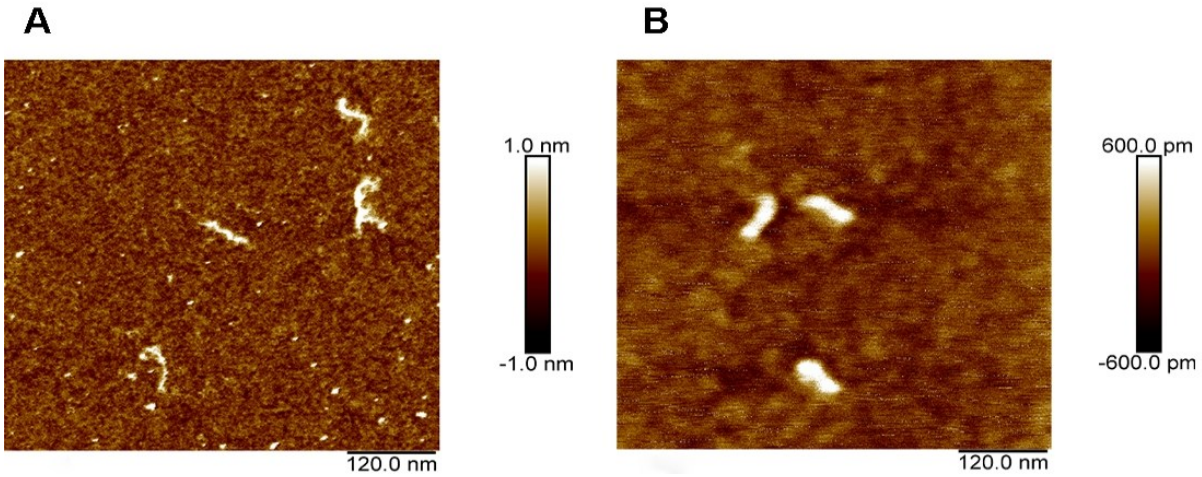

Figure 6 – Stability Assays with decorated nanoparticles. AFM images of particles decorated with: **A)** SpyTag003_sfGFP. **B)** SpyTag003_sfGFP_OVA. In both images, PC ratio = 1 and TC ratio = 0.5.

3.4. Cell Uptake in Immune Cells

Once we demonstrated that the nanoparticles did not lose their features when coated with SpyCatcher003_NucleoX11 and decorated with the SpyTag variants we moved forward to see whether this construction could enter immune cells.

It is well described that size, shape and composition of nanoparticles are important features that determine cell uptake efficiency in eukaryotic cells (Zhang *et al*., 2015; Means *et* al., 2022]. In immune cells specifically, geometry and size are quite important to determine the success in not only cell uptake but also immune activation, once these cells have to deal with a range of pathogens, including the ones that can remodel their own shape (Baranov *et al*., 2021).

Due to this, beside the decorated DNA nanoparticles we also tested the cell uptake of decorated poly I:C RNA particles. Poly I:C is a synthetic analog of dsRNA that carries pathogen-associated molecular patterns (PAMPs) in its sequence (Alexopolou *et al*., 2001). For this study, it was used a commercial mix of low molecular weight dsRNA fragments from InvivoGen® whose average size is 200 bp to 1000 bp, making possible the production of particles with multiple sizes.

It was detected green fluorescence signal inside RAW cells after 24 hours of incubation of these cells with soluble SpyTag003_sfGFP or Nanoparticles decorated with SpyTag003_sfGFP, what indicates that these constructions can internalize macrophages (Fig. 7A).

The results showed on figure 7A indicate that cell uptake occurs not only in a dose-dependent manner but also a in size-dependent manner, since green intracellular fluorescence increases when SpyTag003_sfGFP is attached to particles. This behavior is in accordance with the literature consensus that cell internalization of many small molecules is enhanced when they are carried in nanoplatforms (Wong *et* al., 2013; Mosquera *et al*., 2018; Irvine and Dane, 2020). In fact, calculation models predicts that proteins with 30KDa, like the SpyTag003_sfGFP, have approximately 4 nm of diameter (Erickson, 2009) whereas our DNA particles have around 80 nm of length and RNA particles have an average of 600 nm length.

The effect of decorating particles with the SpyTag003_sfGFP_OVA on cell uptake was also tested. Intracellular fluorescence was measured on DC 2.4 cells, a cloned dendritic cell line that can recognize and present peptides from ovalbumin protein in both MHC-I and MHC-II complexes (Shen *et al*., 1997). This type of cells displayed the same pattern of intracellular green fluorescence enhancement that RAW macrophages (Fig 7B), what indicates that cell uptake of these nanoparticles can occur in distinct immune cell types and this process is not impaired when different decoration is attached.

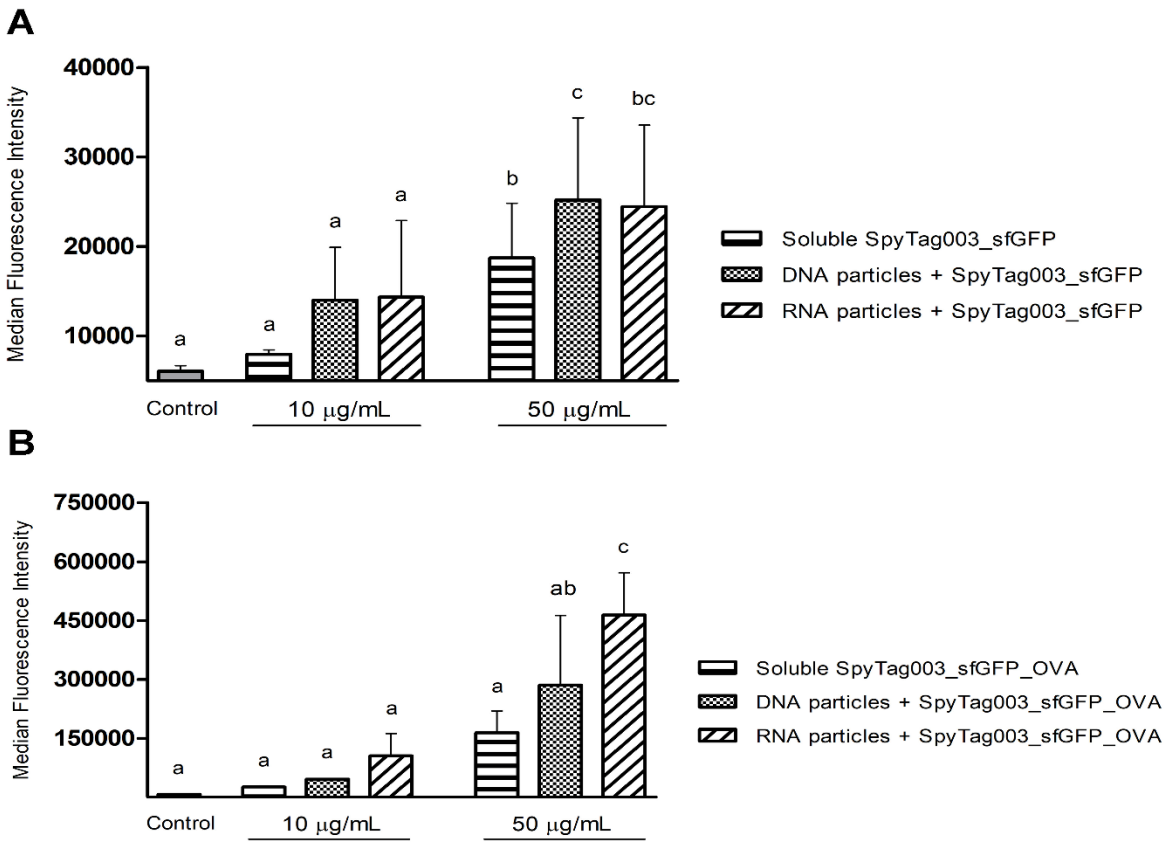

Figure 7 – Cell Uptake in APC: **A)** Macrophages. **B)** Dendritic Cells. Bars represent the average of GFP-MFI extracted from RAW or DC 2.4 cells by flow cytometry after 24 hours of treatment with SpyTag003_sfGFP or SpyTag003_sfGFP_OVA in their soluble form or attached to DNA particles or RNA particles. Control group did not receive any treatment. Error bars represent the standard deviation of three independent experiments. Different letters above the bars represent statistical difference between groups (p-value < 0.05. ANOVA two-way. Bonferroni's test).

3.5. Enhanced expression of CD80 and CD86 on macrophages membranes

The SpyCatcher003_NucleoX11 particles can enter different types of immune cells even when different molecules are attached to them. It reinforces the idea that these stable and cell-suitable particles are a versatile construction that can display different antigens in its surface, what makes it a potential vaccine platform. Due to this we investigated whether these particles could trigger immune responses on macrophages.

Thus, we checked the expression of the membrane proteins CD80 and CD86 on RAW macrophages. These proteins are immunogenic markers that have an important role in immune cells activation in response to antigens, acting as co-stimulatory molecules of the antigen presentation process on APC (Peach *et al*., 1995). The upregulation of CD80 and CD86 on APC is an essential process on lymphocytes activation and consequent initiation of immune

response cascade, since peptide presentation via MHC without sufficient co-stimulation can induces an anergic state in T cells (Alegre *et* al., 2001; Wosen *et al.*, 2018).

It was observed an increase in intracellular signal from anti-CD80 and anti-CD86 antibodies when cells were treated with soluble SpyTag003_sfGFP or nanoparticles decorated with SpyTag003_sfGFP for 24 hours (Fig. 8).

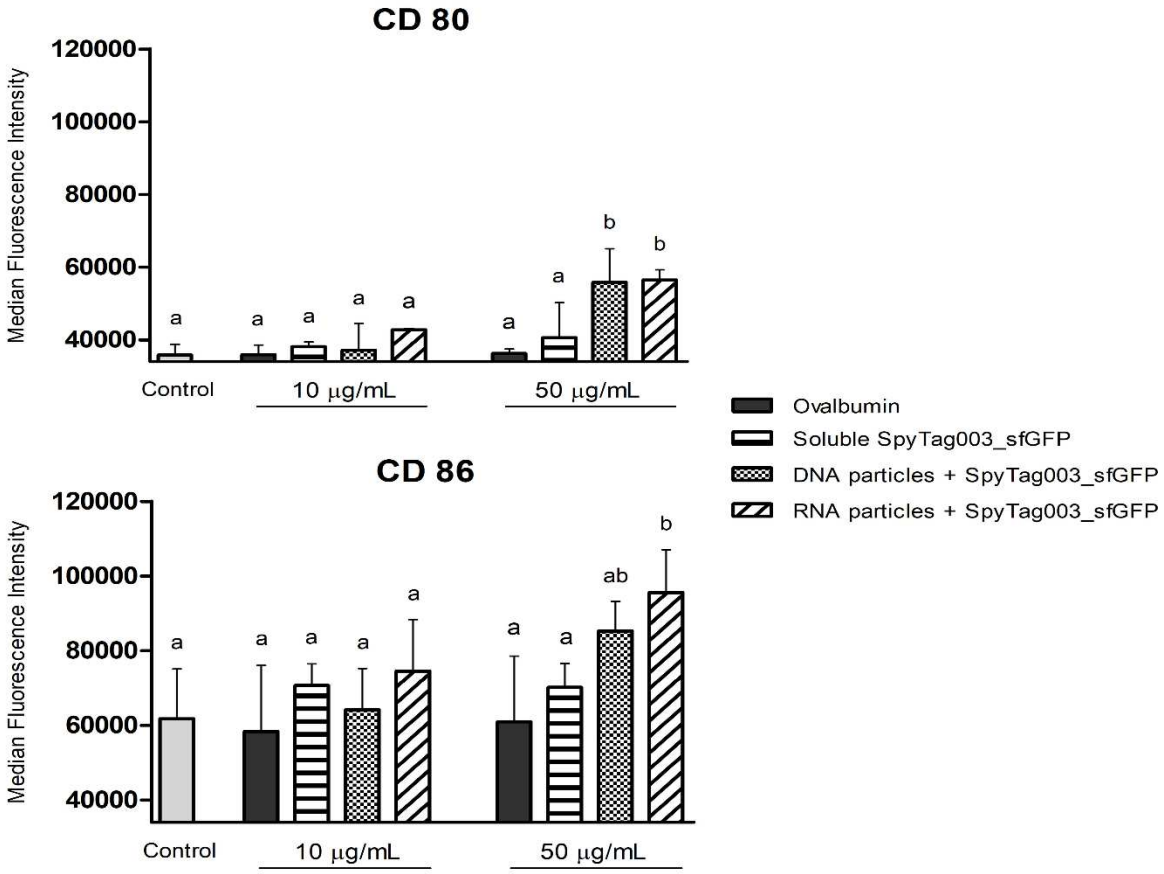

Figure 8 – Expression of CD80 and CD86 in Macrophages. Bars represent the average of PB-MFI (CD80) and PE-MFI (CD86) extracted from RAW cells by flow cytometry after 24 hours of treatment with SpyTag003_sfGFP in its soluble form or attached to DNA particles or RNA particles. Ovalbumin solution was used as a positive control of CD80 and CD86 stimulation. Control group did not receive any treatment. Error bars represent the standard deviation of three independent experiments. Different letters above the bars represent statistical difference between groups (p-value < 0.05. ANOVA two-way. Bonferroni's test).

Similar to cell-uptake, macrophage stimulation upon nanoparticles treatment seems to occur in a dose and composition dependent manner, since SpyTag_sfGFP triggers better immune response when attached to nanoparticles surface and in higher concentrations. However, beside DNA and RNA particles could equally enter macrophage cells when displaying 50 μg/mL of SpyTag_sfGFP in their surfaces (Fig. 7A), only RNA particles, at the same concentration, could significantly trigger CD80 and CD86 expression on RAW cells

surface (Fig. 8). This exclusive response upon RNA particles treatment is probably related to their own composition, once the poly I:C dsRNA here used as particle scaffold can be recognized as PAMPs by immune cells (Fortier *et al.*, 2004). Thus, we can affirm that SpyCatcher_NucleoX11 coating of these particles not only allows the attaching of different antigens via SpyCacther/SpyTag system but also preserves the intrinsic immunogenicity of their nanoparticles scaffold.

Interestingly, ovalbumin solution, a model protein commonly used to sensitize immune responses in mice (Han *et al.*, 2014; Zhang *et al.*, 2017), did not induce expression of CD80 and CD86 molecules at the tested concentrations (Fig. 8). Ovalbumin immunogenic effect only could be observed at 10-fold higher concentrations (data not showed), what indicates that these nanoparticles could trigger immune responses on macrophages more efficiently.

4. Conclusions

Our results show that the SpyCatcher003 peptide can be inserted on N-terminus of NucleoX11 protein without changing its natural functionality and stability, allowing the production of versatile nucleic acid-based nanoparticles that can display a range of peptides containing an SpyTag003 domain. The displaying of fluorescent peptides on SpyCatcher0003_NucleoX11 particles showed that the construction can successfully enter macrophages and dendritic cells and that presentation of these smaller peptides on nanoparticles surface enhances both cell uptake and CD80 and CD86 simulation processes on APC. Besides that, the SpyCatcher003_NucleoX11 coating on nanoparticles preserved intrinsic immunogenicity of nanoparticles scaffold, especially the Poly I:C dsRNA. These data showed that our construction is stable, cell suitable and could be used as an adjuvant platform that can virtually display a range of peptides in its surface, suggesting that SpyCatcher003_NucleoX11 nanoparticles can be a potential vaccine platform.

Author Contributions: A. P. G., and R. H. conducted the experiments and analyzed the data. A. P. G wrote the manuscript. A. A. S., E. T. and R. V. validated the data, reviewed/edited the text and provided/administered resources. All authors have read and agreed to the published version of the manuscript.

Funding: This study was financially supported by the Brazilian agency CAPES and the Dutch agency VLAG.

Acknowledgements: The authors would like to acknowledge the Departments of General Biology and Physics from the Federal University of Viçosa - Brazil and the Physical Chemical Group and the Cell Biology and Immunology Group from the Wageningen University and Research - The Netherlands, for providing the necessary experimental and technical support.

Conflicts of Interest: The authors declare no conflict of interest.

References

AL-BARWANI, F. et al. Mannosylation of virus-like particles enhances internalization by antigen presenting cells. **PloS one**, v. 9, n. 8, p. e104523, 2014.

ALEGRE, M.-L.; FRAUWIRTH, K. A.; THOMPSON, C. B. T-cell regulation by CD28 and CTLA-4. **Nature reviews. Immunology**, v. 1, n. 3, p. 220–228, 2001.

ALEXOPOULOU, L. et al. Recognition of double-stranded RNA and activation of NF-κB by Toll-like receptor 3. **Nature**, v. 413, n. 6857, p. 732–738, 2001.

BARANOV, M. V. et al. Modulation of immune responses by particle size and shape. **Frontiers in immunology**, v. 11, p. 607945, 2021.

BRUNE, K. D. et al. Plug-and-Display: decoration of Virus-Like Particles via isopeptide bonds for modular immunization. **Scientific reports**, v. 6, n. 1, p. 19234, 2016.

DERSH, D.; YEWDELL, J. W.; WEI, J. A SIINFEKL-based system to measure MHC class I antigen presentation efficiency and kinetics. Em: **Antigen Processing**. New York, NY: Springer New York, 2019. p. 109–122.

ERICKSON, H. P. Size and shape of protein molecules at the nanometer level determined by sedimentation, gel filtration, and electron microscopy. **Biological procedures online**, v. 11, n. 1, p. 32–51, 2009.

FORTIER, M.-E. et al. The viral mimic, polyinosinic:polycytidylic acid, induces fever in rats via an interleukin-1-dependent mechanism. **American journal of physiology. Regulatory, integrative and comparative physiology**, v. 287, n. 4, p. R759–R766, 2004.

HALWANI, A. A. Development of pharmaceutical nanomedicines: From the bench to the market. **Pharmaceutics**, v. 14, n. 1, p. 106, 2022.

HAN, J.-A. et al. Ferritin protein cage nanoparticles as versatile antigen delivery nanoplatforms for dendritic cell (DC)-based vaccine development. **Nanomedicine: nanotechnology, biology, and medicine**, v. 10, n. 3, p. 561–569, 2014.

HEDDLE, J. G.; CHAKRABORTI, S.; IWASAKI, K. Natural and artificial protein cages: design, structure and therapeutic applications. **Current opinion in structural biology**, v. 43, p. 148–155, 2017.

HEINIMÄKI, S. et al. Antigenicity and immunogenicity of HA2 and M2e influenza virus antigens conjugated to norovirus-like, VP1 capsid-based particles by the SpyTag/SpyCatcher technology. **Virology**, v. 566, p. 89–97, 2022.

INABA, H.; MATSUURA, K. Peptide nanomaterials designed from natural supramolecular systems. **Chemical record (New York, N.Y.)**, v. 19, n. 5, p. 843–858, 2019.

IRVINE, D. J.; DANE, E. L. Enhancing cancer immunotherapy with nanomedicine. **Nature reviews. Immunology**, v. 20, n. 5, p. 321–334, 2020.

JENNIFER Y., ZHANG J.Y. (2017). Chapter 15-Animal Models of Skin Disorders, **Models for the Study of Human Disease (Second Edition).** Academic Press, p. 357-375.

JOHNSEN, G.; ELSAYED, S. Antigenic and allergenic determinants of ovalbumin—III. MHC Ia-binding peptide (OA 323–339) interacts with human and rabbit specific antibodies. **Molecular immunology**, v. 27, n. 9, p. 821–827, 1990.

MAGINNIS, M. S. Virus–receptor interactions: The key to cellular invasion. **Journal of molecular biology**, v. 430, n. 17, p. 2590–2611, 2018.

MEANS, N. et al. Revealing macropinocytosis using nanoparticles. **Molecular aspects of medicine**, v. 83, n. 100993, p. 100993, 2022.

MOSQUERA, J.; GARCÍA, I.; LIZ-MARZÁN, L. M. Cellular uptake of nanoparticles versus small molecules: A matter of size. **Accounts of chemical research**, v. 51, n. 9, p. 2305–2313, 2018.

MURPHY, J.; CARR, B.; ATKINSON, T. Nanotechnology in medicine and the biosciences. **Trends in biotechnology**, v. 12, n. 8, p. 289–290, 1994.

PEACH, R. J. et al. Both extracellular immunoglobin-like domains of CD80 contain residues critical for binding T cell surface receptors CTLA-4 and CD28. **The journal of biological chemistry**, v. 270, n. 36, p. 21181–21187, 1995.

ROLDÃO, A. et al. Virus-like particles in vaccine development. **Expert review of vaccines**, v. 9, n. 10, p. 1149–1176, 2010.

SHEN, Z. et al. Cloned dendritic cells can present exogenous antigens on both MHC class I and class II molecules. **The journal of immunology**, v. 158, n. 6, p. 2723-2730, 1997.

THRANE, S. et al. Bacterial superglue enables easy development of efficient virus-like particle based vaccines. **Journal of nanobiotechnology**, v. 14, n. 30, 2016.

VEGGIANI, G.; ZAKERI, B.; HOWARTH, M. Superglue from bacteria: unbreakable bridges for protein nanotechnology. **Trends in biotechnology**, v. 32, n. 10, p. 506–512, 2014.

WONG, B. S. et al. Carbon nanotubes for delivery of small molecule drugs. **Advanced drug delivery reviews**, v. 65, n. 15, p. 1964–2015, 2013.

WOSEN, J. E. et al. Epithelial MHC class II expression and its role in antigen presentation in the gastrointestinal and respiratory tracts. **Frontiers in immunology**, v. 9, p. 2144, 2018.

ZAKERI, B. et al. Peptide tag forming a rapid covalent bond to a protein, through engineering a bacterial adhesin. **Proceedings of the National Academy of Sciences of the United States of America**, v. 109, n. 12, p. E690-E697, 2012.

ZEPEDA-CERVANTES, J.; RAMÍREZ-JARQUÍN, J. O.; VACA, L. Interaction between virus-like particles (VLPs) and pattern recognition receptors (PRRs) from dendritic cells (DCs): Toward better engineering of VLPs. **Frontiers in immunology**, v. 11, p. 1100, 2020.

ZHANG, S.; GAO, H.; BAO, G. Physical principles of nanoparticle cellular endocytosis. **ACS nano**, v. 9, n. 9, p. 8655–8671, 2015.

ZHANG J. Market Analysis for Nanomaterials 2020. **Journal of Nanoscience & Nanotechnology Research**, v. 3, n. 2, 2019.

4. CHAPTER 3

CHEMOTHERAPEUTIC-DELIVERING PARTICLES DECORATED WITH ANTI-EGFR NANOBODY REDUCE CELL VIABILITY OF G12V KRAS-POSITIVE COLORECTAL CANCER CELLS

Chemotherapeutic-delivering particles decorated with anti-EGFR nanobody reduce cell viability of G12V *KRAS*-positive colorectal cancer cells

Amanda P. Gonçalves[1], Rob de Haas[2], Leandro Licursi[1], Albert P. Franklin[3], Thanyanne R. M. Ferreira[1], Mariá Braga[3], Marcela Hauck[3], Patrícia Valente[1], Franciele Filardi[1], Renko de Vries[2] & Anésia Santos[1]

1 Department of General Biology, Federal University of Viçosa, Viçosa, 36570-900, Minas Gerais, Brazil
2 Department of Physical Chemistry and Soft Matter, Agrotechnology & Food Sciences Group, Wageningen University and Research, Wageningen, 6708 WE, Gelderland, The Netherlands
3 Department of Biochemistry and Molecular Biology, Federal University of Viçosa, Viçosa, 36570-900, Minas Gerais, Brazil

Abstract

The overexpression of the epidermal growth factor receptor (EGFR) protein on cells surface is a pattern regularly observed in colorectal cancer (CRC), what makes EGFR an important target in CRC treatment. Considering this, we aimed to construct a new drug-delivering platform that exhibits EGFR-ligands in its surface and to evaluate its cytotoxic effects upon EGFR-positive and G12V *KRAS* mutation-bearing CRC cells (SW480). We successfully purified a protein that contains a domain called 7D12, a previously developed anti-EGFR nanobody. The 7D12-bearing protein was conjugated to doxorubicin-carrying particles using the Spy Catcher/Spy Tag technology. It was observed that cell viability of SW480 was reduced in a stronger manner when treated with particles that exhibits 7D12 in their surface, whether compared to cells treated with non-decorated particles. This effect, however, was directly related to the size of particles. The observed reduction on cell viability of CRC cells bearing a mutation related to bad responsiveness to anti-EGFR treatments suggests that our construction can overcome resistance and using anti-EGFR nanobodies as targeting motifs can be a great strategy on drug-delivering of chemotherapeutics in CRC context

Key-words: EGFR targeting; Colorectal cancer; Drug-delivering; Nanobody; Doxorubicin particles.

1. Introduction

Colorectal cancer (CRC) is the third most common cancer worldwide and the fourth most incident neoplasm in Brazil (Morgan *et al.*, 2023; Brazil, 2022). Although global CRC incidence rates had decreased in the last decade, its incidence in transitioning countries and among people younger than 50 years had significantly increased (Morgan *et al.*, 2023).

A commonly observed pattern in CRC is the overexpression of the epidermal growth factor receptor (EGFR). Due to this, EGFR has been pointed as a promising target in CRC treatment (Mendelsohn & Baselga, 2000; Shigeta *et al.*, 2013).

EGFR is a transmembrane tyrosine kinase receptor whose activation is mediated by the binding of specific ligands such as epidermal growth factor (EGF) and transforming growth factor alpha (TGF-α) (Sabbah *et al*., 2020). The EGFR-ligand binding promotes EGFR-dimerization in cell membrane and initiation of phosphorylation-depending cell pathways involved in cell proliferation, migration and apoptosis (Heldin, 1995; Sabbah *et al*., 2020). Due to this, EGFR inhibitors are promising agents for targeted therapy in CRC (Xie *et al*, 2020).

In fact, EGFR-blocking monoclonal antibodies (mAb) such as cetuximab and panitumumab are approved agents that can be used as main therapy or as an adjuvant in CRC treatment (Rocha-Lima *et al.*, 2007; Xie *et al.*, 2020). Unfortunately, these agents present limited efficacy. Around 25% of CRC patients treated with cetuximab are not responders and this rate can lead to 50%. This poor response to treatment is usually related to the presence of mutations in EGFR itself or in important oncogenes such as *KRAF* and *BRAF* (De Roock *et al.*, 2010; Lamtha *et al.*, 2022). Thus, the search for effective EGFR-targeting molecules that overcomes resistance in mutated CRC cells is still necessary.

One promising alternative is the clinical use of a distinct class of antibodies known as nanobodies. Nanobodies, also called VHHs, are naturally found in Camelidae, formed by a single heavy-chain variable domain. Due to this, they present a very reduced size and molecular weight (Roovers *et al*., 2007). Despite their reduced size and complexity, VHHs antigen-binding is as effective as regular antibodies. Furthermore, they can exhibit better stability and solubility in physiological conditions (Bao *et al.*, 2021; Muyldermans, 2021).

The importance that EGFR plays in solid tumors makes the developing of anti-EGFR VHHs a hot topic. In 2005, the use of anti-EGFR in the treatment of xenograft solid tumors was reported for the first time (Roovers *et al*., 2007). Currently, a range of these products are

being developed as target-therapy alternatives, but all of them are still in a first experimental phase (Sharifi *et al.*, 2021).

Our search for studies using anti-EGFR VHHs applied exclusively to CRC treatment has returned interesting studies (see Figure 1 and Table 1). The number of these studies however is not high, suggesting that this is still an open field that needs to be explored.

Considering that, in this study we aimed to produce nanoparticles that exhibits anti-EGFR VHHs in their surface as well as to evaluate their use as adjuvants in the treatment of EGFR-positive CRC cells (SW480) with doxorubicin (DOX). To achieve this, we used the Spy Catcher/Spy Tag technology (Zakeri *et al.*, 2012) to conjugate the anti-EGFR VHH 7D12 (Gainkam *et al.,* 2008) to the previously developed virus-like self-assembling protein Spy_NucleoX11 (see chapter 2), producing the Spy_7D12 particles. The effect of Spy_7D12 carrying DOX upon SW480 cells was evaluated by *in vitro* cell assays.

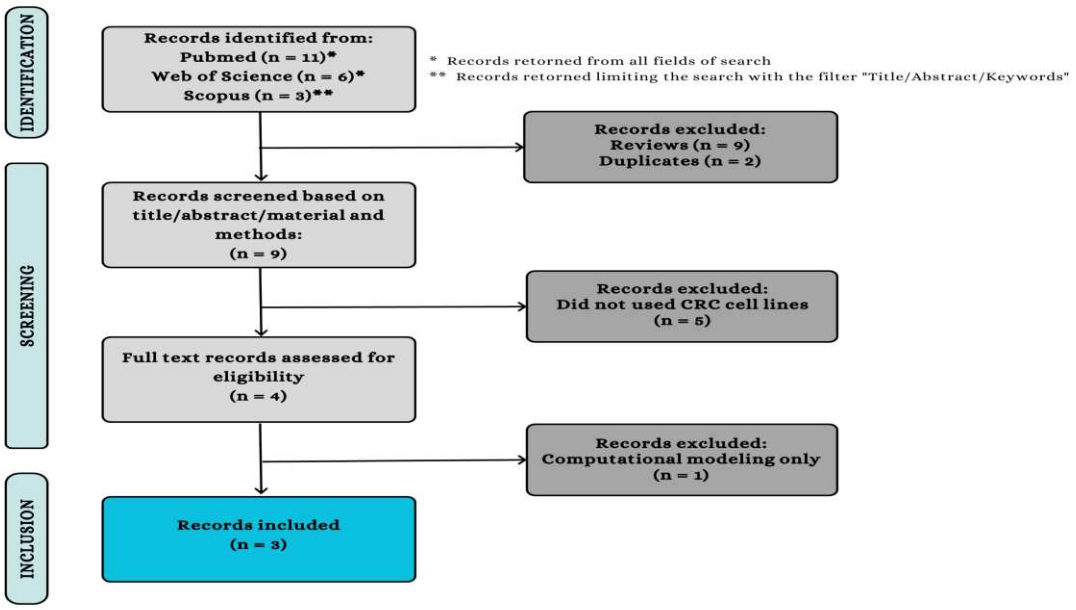

Figure 1: Search strategy used to find records relating the use of anti-EGFR VHHs applied to CRC treatment. The search was conducted in Pubmed, Web of Science and Scopus databases by typing the following term in the query box: "((colorectal cancer OR rectal cancer OR colon cancer OR bowel cancer) AND (EGF receptor OR anti-EGFR) AND (nanobody OR nanobodies))". Research articles published after August 1st, 2023 are not included.

Table 1: Anti-EGFR VHHs applied to CRC treatment.

REFERENCE	CONSTRUCTION NAME	THERAPY NATURE	CRC CELL LINES	IN VIVO STUDIES	OBSERVED EFFECT
de Bruin *et al*., 2018.	7D12-5GS-6H4.	Combined therapy: bi-specific VHH (anti-EGFR 7D12 + anti-Vδ2 6H4) and Vγ9Vδ2-T cells.	SW480, HT-29 and primary CRC cells.	Yes.	Increase on Vγ9Vδ2-T cells activation, cytotoxic granules release and CRC cell lysis.
Lamtha *et al*., 2022	R9VH36.	Main therapy: anti-EGFR VHH only.	SW480	No.	Decrease on CRC cell viability; Changes in proteomic profile.
Narbona *et al*., 2023	V_{HH}EGFRαS and BsITXαSDI.	Combined therapy: anti-EGFR 7D12 and immunotoxin (α-sarcin) OR anti-EGFR 7D12, anti-GPA33 and α-sarcin.	SW1222	Yes.	Decrease on CRC cell viability; Improve on mice survival rate.

2. Material and Methods

2.1. Plasmid construction

The expression vector of SpyNucleoX11protein were previously obtained, as described in Chapter 2 (section 2.1, page 33).

The expression vector of SpyTag_sfGFP_7D12 protein was purchased from Twist Bioscience. The DNA sequence encoding the protein of interest was inserted into the pET-29b+ vector, between the restriction sites Ndel and Xhol. The DNA sequence that encodes the SpyTag_sfGFP_7D12 protein was designed in the software Snap Gene 5.0.8. Encoding sequences of SpyTag003 peptide, sfGFP protein and 7D12 anti-EGFR VHH are public and can be consulted in *Keeble et al., 2019*, *Pédelacq et al., 2006* and *Gainkam et al., 2008*, respectively.

2.2. Protein expression

SpyNucleoX11 protein was obtained by IMAC protein purification, as described in Chapter 2 (section 2.2, page 33).

SpyTag_sfGFP_7D12 protein was also obtained by IMAC protein purification, using a gravity column loaded with nickel-charged resin. Salt and contaminants were removed by dialysis using PBS pH 7.4 and a 10 kDa MWCO centrifugal concentrator. Final product was stored at –20°C diluted in PBS pH 7.4 + 10% glycerol.

2.3. SpyNucleoX11 and SpyTag_sfGFP_7D12 protein coupling

The two proteins were incubate together for 24 hours at room temperature in SpyNucleoX11/SpyTag_sfGFP_7D12 molar ratios of 1:1, 1:3 and 1:5. These ratios were obtained by mixing 3 µL of SpyNucleoX11 [29 µM] with 13.5 µL, 40.5 µL or 67.5 µL of SpyTag_sfGFP_7D12 [6.45 µM], respectively. Coupling efficiency was checked by denaturing SDS page.

2.4. Self-assembly of DOX-loaded nanoparticles

DOX-loaded nanoparticles were assembled by mixing 4 µL of dsDNA fragments [100 ng/ µL] and 34 µL of DOX [440 nM]. The mixture was incubated in a dark tube at room temperature for 1 h to allow DOX intercalation. Small particles were assembled using 600 bp DNA fragments and large particles were assembled using 3000 bp DNA fragments. DNA fragments and DOX Hydrochloride were purchased from Thermo Fisher® and Sigma Aldrich®, respectively.

To generate non-decorated particles, 3 µL of SpyNucleoX11 [29 µM] were added to DNA-DOX complexes. Then, this mixture was incubated in the dark for 24 hours at room temperature. To generate particles decorated with anti-EGFR VHHs, 16.5 µL of coupled SpyNucleoX11/SpyTag_sfGFP_7D12 product, in a 1:1 molar ratio, were added to DNA-DOX complexes. Then, this mixture was incubated as described above.

2.5. Cell culture

CRC cell line SW480 was kindly donated by Professor Gustavo Bressan (Molecular Biology Laboratory, Federal University of Viçosa, Minas Gerais, Brazil). Cells were cultured in 25 cm^2 plastic flasks containing RPMI-1640 medium supplemented with 10% of fetal bovine serum, 0.2% of D-glucose, 0.1% of antibiotics (penicillin and streptomycin), 0.03% of L-glutamine and 0.025% of antimycotic (amphotericin B). Cell were incubated at controlled temperature (37ºC) and atmosphere (5% of CO_2).

2.6. Cell proliferation assay

SW480 cells were seeded in 96-wells plates ($1x10^4$ cells/well) and allowed to attach for 24 hours at the conditions described above. The next day, fresh medium was replaced with media + EGF (100 µL/well) in different concentrations of EGF (50 nM, 25 nM, 12.5 nM, 6.3 nM, 3.1 nM, 1.6 nM, 0.8 nM, 0.4 nM and 0.2 nM), obtained by serial dilution. After 48 or 72 hours, cell viability of SW480 under different conditions was assessed by MTT assay (Mosmann, 1983). Media + EGF was replaced with media supplemented with 10% of MTT [0.5 mg/mL] (50 µL/well) and cells were incubated at 37ºC for 3 hours. Next, supernatant was removed and the formazan crystals formed during MTT reaction were dissolved with DMSO (50 µL/well). Then, absorbance was measured at 570 nm using a microplate reader (SpectraMax®).

2.7. Cytotoxicity assay

96-wells plates of SW480 cells were prepared as described above. The next day, fresh medium was replaced with media + DOX (100 µL/well) in different concentrations of DOX (10 µM, 5 µM and 2.5 µM), with media + SpyTag_sfGFP_7D12 (60 nM, 30 nM and 15 nM) or with media + non-loaded particles (60 nM, 30 nM and 15 nM of SpyTag_sfGFP_7D12). After 72 hours, cell viability of SW480 cells was also assessed by MTT assay, as described above.

2.8. Half-Maximum Inhibitory Concentration (IC_{50}) Calculation

IC_{50} values of the different treatments were determined by non-linear regression of the logarithmic dose of treatment *versus* normalized response (% of cell viability). Data was analyzed in the software GraphPad Prism 5.0.

2.9. Statistical Analysis

Graphs and statistical analysis were also performed in GraphPad Prism 5.0. Experimental data were extracted from three or four independent experiments. Statistical tests are mentioned in figures' caption and p-values < 0.05 were considered statistically significant.

3. Results

3.1. Generation of the peptide SpyTag_sfGFP_7D12

Since we wanted to use the anti-EGFR VHHs to decorate the surface of nanoparticles coated with the Spy_NucleoX11 protein, a virus-like protein that contains a SpyCatcher domain in its N-terminus (see chapter 2), we generated a new construction conjugating the Spy Tag 003 peptide with the protein sfGFP and the anti-EGFR VHH 7D12, which we called SpyTag_sfGFP_7D12 . The Spy Tag domain is located in the N-terminus and the three different portions are linked by small flexible Gly-Ser linkers (Figure 2). The sfGFP domain was included to generate a fluorescent construction that can be tracked in cellular assays.

Figure 2: Schematic diagram representing domain distribution of SpyTag_sfGFP_7D12 protein. SpyTag, sfGFP and 7D12 domains are linked by a 6-amino acids Gly-Ser linker. SpyTag domain is positioned at N-terminus and a nickel-affinity His-Tag at C-terminus.

The SpyTag_sfGFP_7D12 sequence has 399 amino acids and an estimated molecular weight of 43.95 KDa (Supplementary Information, Table 1). After IMAC protein purification, we obtained a product of approximately 40 KDa with Spy Catcher-binding activity, confirmed by SDS Page coupling assay (Figure 3), what suggests that the SpyTag_sfGFP_7D12 protein was successfully obtained.

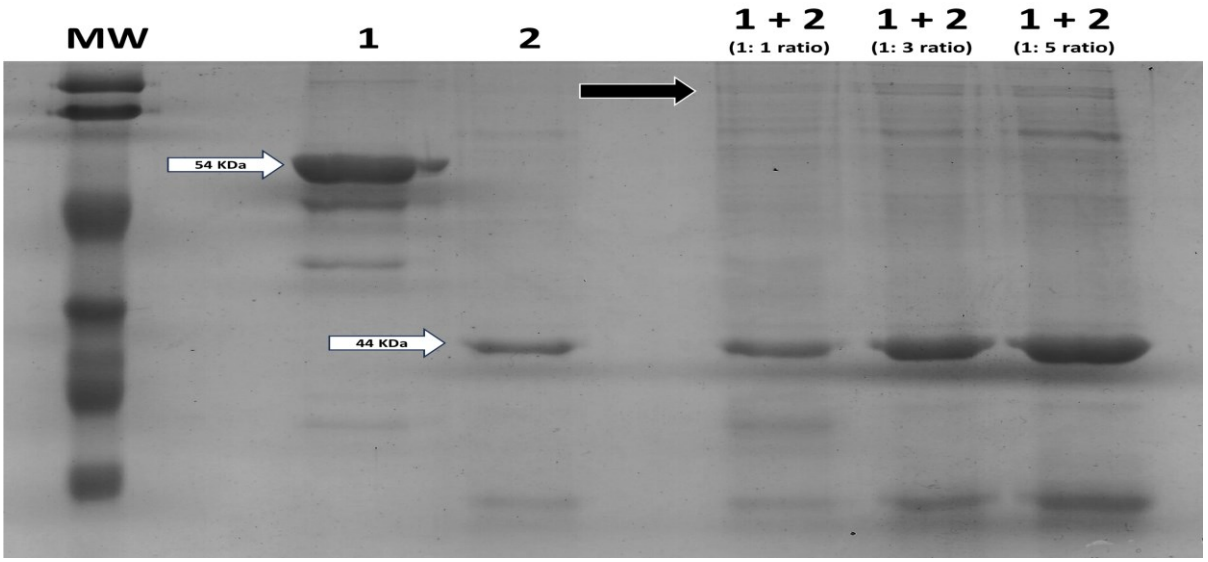

Figure 3: SDS Page and Coupling Assay. SDS-Page of a 10% polyacrylamide gel performed after IMAC purification of SpyTag_sfGFP_7D12. MW represents the standard molecular weight marker; 1 and 2 represent SpyNucleoX11 and SpyTag_sfGFP_7D12, respectively. A new product with a higher molecular weight is formed when we mix 1 and 2 in different ratios (see black arrow), indicating the proper coupling of SpyNucleoX11 and SpyTag_sfGFP_7D12.

3.2. SW480 cell response to EGF

Since SW480 cells is an EGFR-positive cell line (Shigeta *et al*., 2013; Digre and Lindskog, 2023) and EGF/EGFR binding is related to an increase in cell proliferation (Yarden and Sliwkowski, 2001), we measured cell proliferation of SW480 cells treated with different concentrations of EGF by MTT assay. As expected, SW480 cells treated with EGF for 72 hours presented increased cell proliferation rates (Figure 4). The pattern observed, however, suggests that EGF effect upon SW480 cells is not dependent of concentration doses, but of time of treatment, since cell treated with EGF for 48 hours did not showed increased cell proliferation rates.

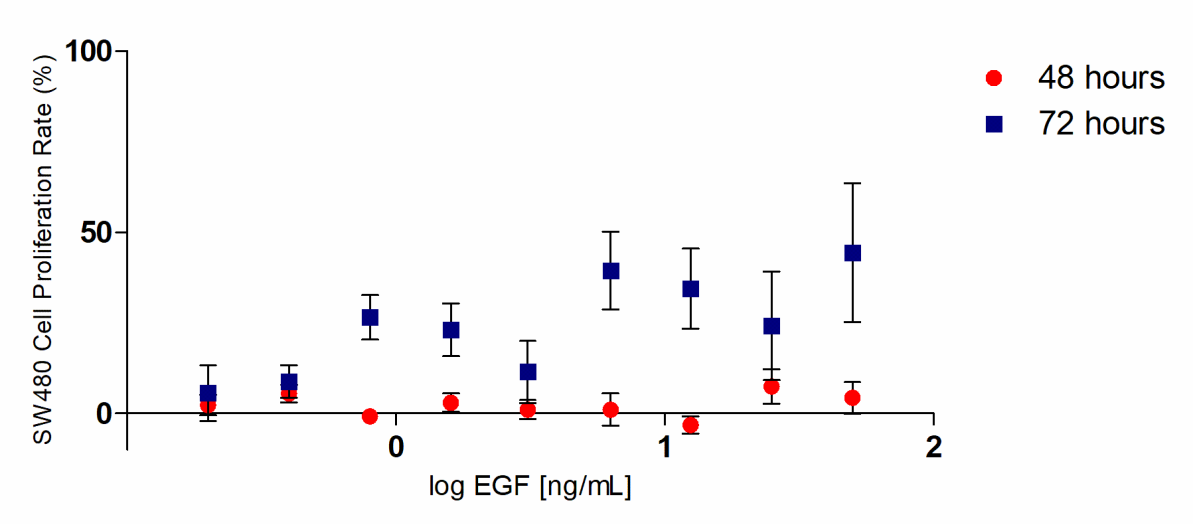

Figure 4: Cell proliferation rate of SW480 cell treated with EGF. Cells were treated for 48 and 72 hours with different concentrations of EGF. Results are expressed as the mean ± SEM of four independent experiments.

3.3. SW480 cell viability

Cell viability of SW480 cells treated with encapsulated DOX (Spy_DOX) or encapsulated DOX conjugated with anti-EGFR nanobody (Spy_DOX_7D12) was also evaluated by MTT assay. Two different sizes of Spy_DOX or Spy_DOX_7D12 particles were offered to cells to determine whether particles size can interfere on treatment efficacy. After 72h of treatment, SW480 showed significant decrease in cell viability in a dose-dependent manner (Figure 5), but this does not occur when cells are treated with non-loaded particles or with SpyTag_sfGFP_7D12 (Figure 6), what suggests that the delivery platform is cytotoxic only when loaded with DOX.

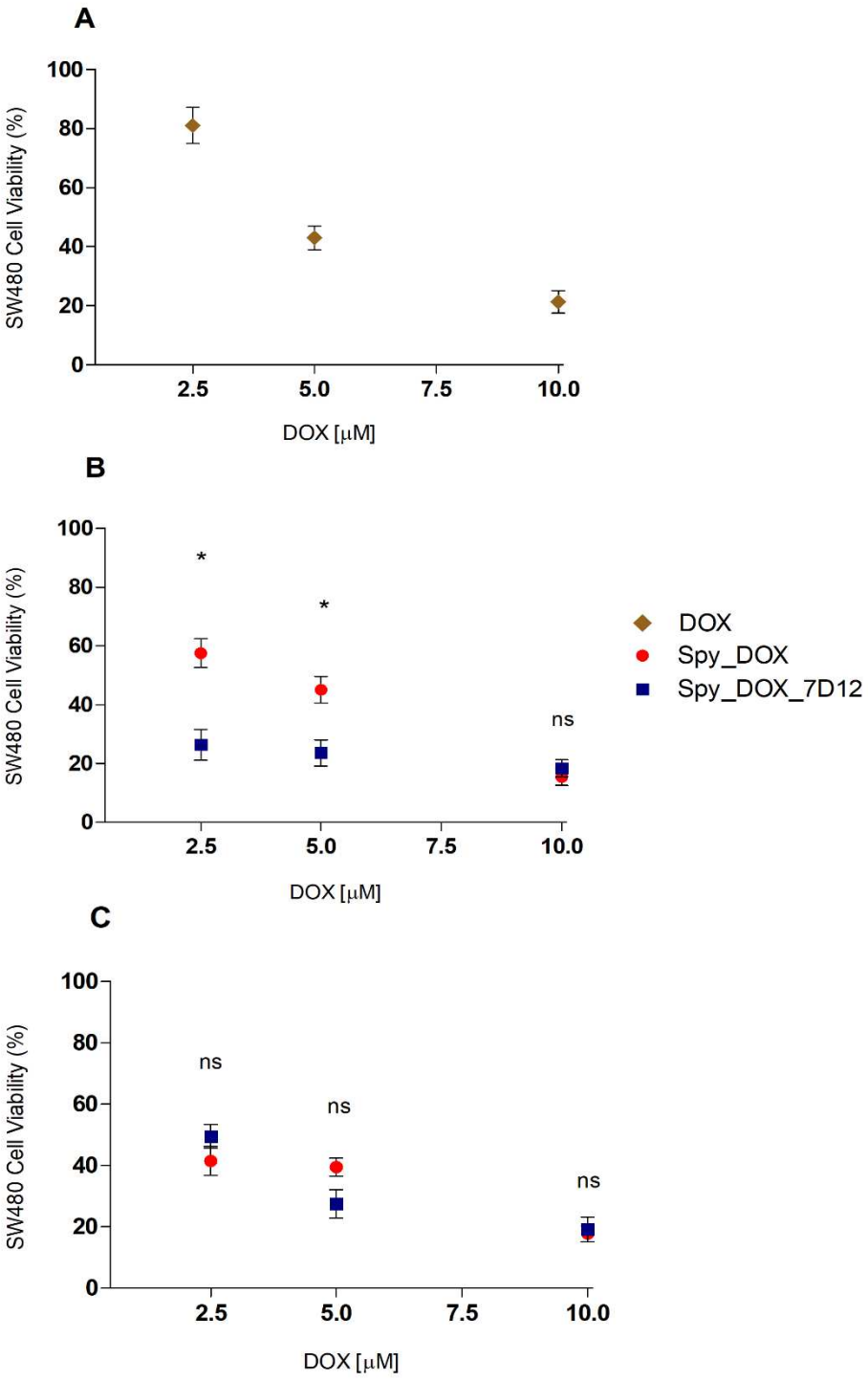

Figure 5: SW480 cell viability after treatment with free DOX or DOX-loaded particles. Cells were treated for 72 hours with non-encapsulated DOX (A) and large particles (B) or small particles (C) of Spy_DOX or Spy_DOX_7D12. Results are expressed as the mean ± SEM of three independent experiments. Asterisks represent a p-value < 0.05, calculated with a one-way ANOVA and Tukey's post-hoc test.

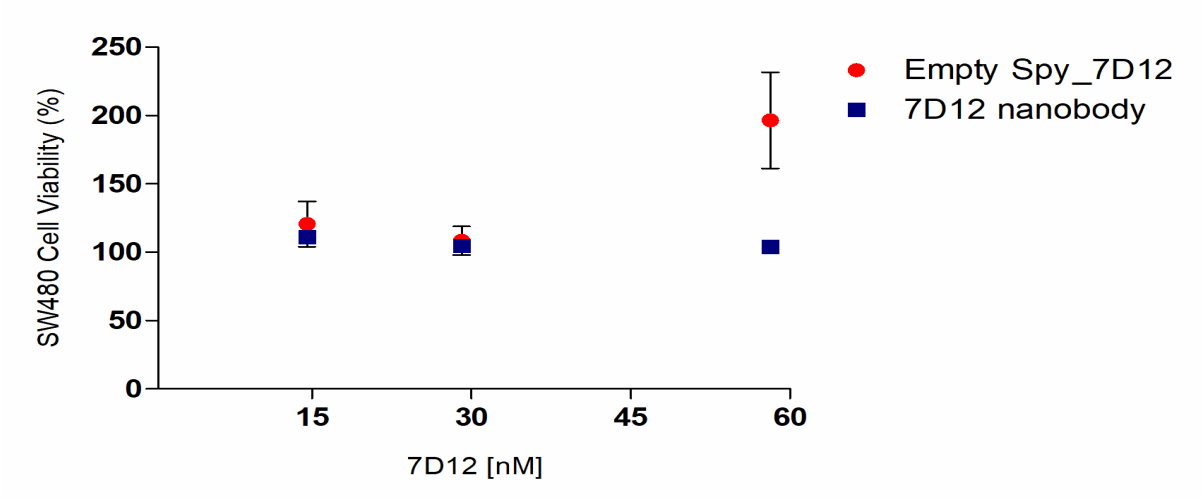

Figure 6: SW480 cell viability after treatment with non-loaded particles. Cells were treated for 72 hours with non-loaded decorated particles and 7D12 VHH only. Results are expressed as the mean ± SEM of three independent experiments.

Spy_DOX_7D12 treatment using large particles offered a two-fold decrease in cell viability of SW480 cells when compared to Spy_DOX treatment (Figure 5b). When we used small particles, however, no significant differences between the two treatments were observed (Figure 5c). Nevertheless, Spy_DOX_7D12 treatment offered superior cytotoxicity to SW480 cells, with an IC_{50} value of 0.82 µM, the smallest among the observed treatments (Table 2). In fact, delivering DOX in particles reduced IC_{50} values in all the tested conditions, even when particles did not display 7D12 peptides in their surfaces.

Table 2: IC50 values of DOX delivered to SW480 cells in its free form and in large or small particles of Spy_DOX and Spy_DOX_7D12.

	FREE DOX	**SPY_DOX**	**SPY_DOX_7D12**
NO PARTICLES	4.59 ± 1.38 µM ($R^2 = 0.72$)	-	-
LARGE PARTICLES	-	4.04 ± 0.46 µM ($R^2 = 0.91$)	0.82 ± 0.58 µM ($R^2 = 0.87$)
SMALL PARTICLES	-	1.95 ± 0.72 µM ($R^2 = 0.83$)	2.35 ± 0.63 µM ($R^2 = 0.81$)

4. Discussion

The use of DNA-based virus-like particles (VLPs) as efficient delivery platforms of DOX is not unprecedented. Here, however, we propose the improvement of this delivery model by decorating the surface of DOX-loaded VLPs with the anti-EGFR VHH 7D12.

Some studies have already show that 7D12 is an efficient tumor cell inhibitor, acting itself as an antagonist or as part of major structures that target EGFR-positive cancer cells (Roovers *et al*., 2011; Heukers *et al*., 2013). Other types of anti-EGFR VHHs were also used to decorate the surface of liposomes and albumin nanoparticles. Such modifications promoted a better biodistribution and tumor penetration of these constructions (Kijanka *et al*., 2015). Nevertheless, we have not found studies using VLPs decorated with 7D12 or other anti-EGFR VHHs.

As shown in Figure 5b, cell viability of SW480 is highly reduced when large DOX-loaded VLPs are decorated with 7D12. This behavior is not completely unexpected, since SW480 is an EGFR-positive cell. However, SW480 also exhibits the mutation G12V on gene *KRAS* (Berg *et al*., 2017), which is associated with bad responses to anti-EGFR therapies (Alves *et al*., 2015; Lamtha *et al*., 2022). In fact, anti-EGFR mAb treatments such as cetuximab is only recommended to treat patients that bear *KRAS* wild-type EGFR-positive tumor cells (U. S. Food and Drug Administration, 2021). In accordance to this, we showed that empty particles and SpyTag_sfGFP_7D12 did not reduce SW480 cell viability (Figure 6).

In this sense, our results suggests that although 7D12 itself is not able to reduce CRC cell viability, but the delivery of DOX in anti-EGFR decorated particles improves the cytotoxicity of the chemotherapy. This is probably related to a better internalization of the decorated particles in EGFR-positive cells, a behavior already observed by Oliveira *et al*., 2010 and Wang *et al*., 2017. Cell uptake experiments such as flow cytometry and fluorescence microscopy are needed to confirm this hypothesis. Moreover, IC_{50} value of free DOX was higher than all forms of encapsulated DOX (Table 2), demonstrating that delivering DOX in particles can somehow improve its efficacy.

It is also important to highlight that SW480 treated with DOX-loaded particles exhibited different responses, depending on the size of the particles used. Treatment with large anti-EGFR decorated particles triggered higher cell death rates than treatment with small particles (Figure 5). This suggests that decorating DOX particles with 7D12 can be a great strategy to improve cytotoxicity, but the size of the delivery platform is determinant to achieve the best treatment efficiency.

In fact, size is a determinant factor in the successful cell uptake of particles (Leclerc *et al*., 2012; Li *et al*., 2022). Whereas particles larger than 500 nm enter cells by phagocytosis and micropinocytosis, particles around 100 nm enter cells by receptor-mediated mechanisms, such as clathrin and caveolae mediated endocytosis (Kettler *et al*., 2014).

The large particles used in this work were built using 3000 bp DNA molecules as scaffold, what gives them a size of approximately 1 μm, considering that the standard length of a single base pair is 0.34 nm (Alberts *et al*., 2014; Bettotti *et al*., 2018). Although particles of this size did not fit in the nanoscale, Trewyin and colleagues report that functionalized rod-shaped particles with sizes varying between 400 nm and 1 μm can properly enter fibroblasts and tumor cells, with a better uptake rate in the tumoral type (Trewyin *et al*., 2008).

In our case, better internalization of large particles can be related not only to the cell type model or to a distinct cell entrance mechanism, but also to an overstimulation of EGFR pathway in SW480 cells, since large particles can be able to cluster more anti-EGFR VHHs in their surface than smaller ones. This can be further investigated by endocytosis-blocking assays and by tracking the intracellular GFP signal derived from these decorated particles.

In conclusion, the new designed protein SpyTag_sfGFP_7D12 was used to decorate the surface of DOX-loaded VLPs. We showed that decorating particles with anti-EGFR VHHs enhanced the cytotoxicity of DOX-particles upon SW480 cells and this effect is directly dependent of particles size. These results suggest that our construction can overcome resistance in cancer treatment, since the EGFR-positive CRC cells used here bear the G12V *KRAS* mutation, which is strongly related to non-responsiveness to EGFR-targeting treatments. In addition, the results suggest that size of delivering platform must be carefully chosen to achieve better cytotoxicity effects. Investigations related to intracellular DOX release, cell uptake mechanisms and EGFR pathway activation are suggested to fully understand how CRC cells respond to our proposed model of DOX-loaded particles decorated with anti-EGFR VHHs.

Funding: This study was financially supported by the Brazilian agencies CAPES, CNPQ and FAPEMIG.
Acknowledgements: The authors would like to acknowledge the Departments of General Biology and Physics from the Federal University of Viçosa - Brazil and the Physical Chemical Group and Soft Matter group from the Wageningen University and Research - The Netherlands, for providing the necessary experimental and technical support.

Conflicts of Interest: The authors declare no conflict of interest.

References

ALBERTS, B. **Molecular biology of the cell**. 6. ed. Nova Iorque, NY, USA: Garland Publishing, 2014

ALVES, S. et al. Colorectal cancer-related mutant KRAS alleles function as positive regulators of autophagy. **Oncotarget**, v. 6, n. 31, p. 30787–30802, 2015.

BAO, G. et al. Nanobody: a promising toolkit for molecular imaging and disease therapy. EJNMMI Research. **EJNMMI Research**, v. 11, n. 6, 2021.

BERG, K. C. G. et al. Multi-omics of 34 colorectal cancer cell lines - a resource for biomedical studies**. Molecular Cancer**, v. 16, n. 1, 2017.

BETTOTTI, P. et al. Structure and properties of DNA molecules over the full range of biologically relevant supercoiling states. **Scientific reports**, v. 8, n. 1, 2018

BRAZIL, INSTITUTO NACIONAL DO CÂNCER. **Estimativa 2023: Incidência de Câncer no Brasil**. Rio de Janeiro, 2022.

DE BRUIN, R. C. G. et al. A bispecific nanobody approach to leverage the potent and widely applicable tumor cytolytic capacity of Vγ9Vδ2-T cells. **OncoImmunology**, v. 7, n. 1, 2018.

DE ROOCK, W. et al. Effects of KRAS, BRAF, NRAS, and PIK3CA mutations on the efficacy of cetuximab plus chemotherapy in chemotherapy-refractory metastatic colorectal cancer: a retrospective consortium analysis. **Lancet Oncology**, v. 11, p. 753–762, 2010.

DIGRE, A.; LINDSKOG, C. The human protein atlas—Integrated omics for single cell mapping of the human proteome. **Protein Science**, v. 32, n. 2, 2023.

GAINKAM, L. O. T. et al. Comparison of the biodistribution and tumor targeting of two 99mTc-labeled anti-EGFR nanobodies in mice, using pinhole SPECT/micro-CT. **Journal of Nuclear Medicine**, v. 49, n. 5, p. 788–795, 2008.

HELDIN, C-H. Dimerization of Cell Surface Receptors in Signal Transduction. **Cell**, v. 80, p. 213-223, 1995.

KEEBLE, A. H. et al. Approaching infinite affinity through engineering of peptide-protein interaction. **PNAS**, v. 116, n. 52, p. 26523–26533, 2019.

KETTLER, K. et al. Cellular uptake of nanoparticles as determined by particle properties, experimental conditions, and cell type. **Environmental Toxicology and Chemistry**, v. 33, n. 3, p. 481–492, 2014.

KIJANKA, M. et al. **Nanobody-based cancer therapy of solid tumors**. **Nanomedicine (Lond.)**, v. 10(1), p. 161–174, 2015.

LAMTHA, T. et al. A novel nanobody as therapeutics target for EGFR-positive colorectal cancer therapy: exploring the effects of the nanobody on SW480 cells using proteomics approach. **Proteome Science**, v. 20, n. 1, 2022.

LECLERC, L. et al. Size of submicrometric and nanometric particles affect cellular uptake and biological activity of macrophages in vitro. **Inhalation Toxicology**, v. 24, n. 9, p. 580–588, 2012.

LI, X. et al. Design of Smart Size-, Surface-, and Shape-Switching Nanoparticles to Improve Therapeutic Efficacy. **Small,** v.18, p. e2104632, 2022.

MENDELSOHN, J.; BASELGA, J. The EGF receptor family as targets for cancer therapy. **Oncogene**, v. 19, p. 6550–6566, 2000.

MORGAN, E. et al. Global burden of colorectal cancer in 2020 and 2040: Incidence and mortality estimates from GLOBOCAN. **Gut**, v. 72, n. 2, p. 338–344, 2023.

MOSMANN, T. Rapid Colorimetric Assay for Cellular Growth and Survival: Application to Proliferation and Cytotoxicity Assays. **Journal of lmmunological Methods**. v. 65, p. 55-63, 1983

MUYLDERMANS, S. Applications of Nanobodies. **Annual Review of Animal Biosciences**, v. 9, p. 401–421, 2020.

NARBONA, J. et al. Nanobody-Based EGFR-Targeting Immunotoxins for Colorectal Cancer Treatment. **Biomolecules**, v. 13, n. 7, p. 1042, 26 jun. 2023.

OLIVEIRA, S. et al. Downregulation of EGFR by a novel multivalent nanobody-liposome platform. **Journal of Controlled Release**, v. 145, n. 2, p. 165–175, 2010.

PÉDELACQ, J. D. et al. Engineering and characterization of a superfolder green fluorescent protein. **Nature Biotechnology**, v. 24, n. 1, p. 79–88, 2006.

ROCHA-LIMA, C. M. et al. EGFR Targeting of Solid Tumors. **Cancer Control**, v. 14, n. 3, p. 295–304, 2007.

ROOVERS, R. C. et al. Efficient inhibition of EGFR signalling and of tumour growth by antagonistic anti-EGFR Nanobodies. **Cancer Immunology, Immunotherapy**, v. 56, n. 3, p. 303–317, 2007.

ROOVERS, R. C. et al. A biparatopic anti-EGFR nanobody efficiently inhibits solid tumour growth. **International Journal of Cancer**, v. 129, n. 8, p. 2013–2024, 15 out. 2011.

SABBAH, D. A.; HAJJO, R.; SWEIDAN, K. Review on Epidermal Growth Factor Receptor (EGFR) Structure, Signalling Pathways, Interactions, and Recent Updates of EGFR Inhibitors. **Current Topics in Medicinal Chemistry**, v. 20, n. 10, p. 815–834, 3 mar. 2020.

SHARIFI, J. et al. EGFR and anti-EGFR nanobodies: review and update. **Journal of Drug Targeting,** v. 29:4, p. 387-402, 2021.

SHIGETA, K. et al. Expression of Epidermal Growth Factor Receptor Detected by Cetuximab Indicates Its Efficacy to Inhibit In Vitro and In Vivo Proliferation of Colorectal Cancer Cells. **PLoS ONE**, v. 8, n. 6, 2013.

SIEGEL, R. L. et al. Colorectal cancer statistics, 2023. **CA: A Cancer Journal for Clinicians**, v. 73, n. 3, p. 233–254, 2023.

TREWYN, B. G. et al. Biocompatible mesoporous silica nanoparticles with different morphologies for animal cell membrane penetration. **Chemical Engineering Journal**, v. 137, n. 1, p. 23–29, 2008.

U. S. FOOD AND DRUG ADMINISTRATION. **FDA D.I.S.C.O. Burst Edition: FDA approvals of Erbitux (cetuximab) for K-Ras wild type, EGFR-expressing colorectal cancer or squamous cell carcinoma of the head and neck and Trodelvy (sacituzumab govitecan) for patients with unresectable locally advanced or metastatic triple negative breast cancer**. Available at: <https://www.fda.gov/drugs/resources-information-approved-drugs/fda-disco-burst-edition-fda-approvals-erbitux-cetuximab-k-ras-wild-type-egfr-expressing-colorectal>. Access in: Sep 18th, 2023.

WANG, Y. et al. Quantum-Dot-Based Theranostic Micelles Conjugated with an Anti-EGFR Nanobody for Triple-Negative Breast Cancer Therapy. **ACS Applied Materials and Interfaces**, v. 9, n. 36, p. 30297–30305, 2017.

XIE, Y. H.; CHEN, Y. X.; FANG, J. Y. Comprehensive review of targeted therapy for colorectal cancer. **Signal Transduction and Targeted Therapy,** v. 5:22, 2020.

YARDEN, Y.; SLIWKOWSKI, M. X. UNTANGLING THE ErbB SIGNALLING NETWORK. **Nature Reviews | Molecular Cell Biology**, v. 2, p. 127–137, 2001.

ZAKERI, B. et al. Peptide tag forming a rapid covalent bond to a protein, through engineering a bacterial adhesin. **PNAS**, v. 109, n. 12, p. E690–E697, 2012.

SUPPLEMENTARY INFORMATION

Chemotherapeutic-delivering particles decorated with anti-EGFR nanobody reduce cell viability of G12V *KRAS*-positive colorectal cancer cells

Amanda P. Gonçalves[1], Rob de Haas[2], Leandro Licursi[1], Mariá Braga[3], Marcela Hauck[3], Patrícia Valente[1], Franciele Filardi[1], Renko de Vries[2] & Anésia Santos[1]

Table S1: Full amino acids sequence of SpyTag_sfGFP_7D12 protein. Estimated molecular weight = 43952 Da; Total number of amino acids = 399.

MGRGVPHIVMVDAYKRYKSGGGSGRKGEELFTGVVPILVELDGDVNGHKFSVRGEGE
GDATNGKLTLKFICTTGKLPVPWPTLVTTLTYGVQCFARYPDHMKQHDFFKSAMPEGY
VQERTISFKDDGTYKTRAEVKFEGDTLVNRIELKGIDFKEDGNILGHKLEYNFNSHNVYI
TADKQKNGIKANFKIRHNVEDGSVQLADHYQQNTPIGDGPVLLPDNHYLSTQSVLSKD
PNEKRDHMVLLEFVTAAGITHGMDELYKSGGGSGQVKLEESGGGSVQTGGSLRLTCA
ASGRTSRSYGMGWFRQAPGKEREFVSGISWRGDSTGYADSVKGRFTISRDNAKNTVDL
QMNSLKPEDTAIYYCAAAAGSAWYGTLYEYDYWGQGTQVTVSSGSHHHHHH

Color codes: Red: SpyTag003 domain; Green: sfGFP domain; Blue: 7D12 nanobody domain; Orange: HisTag.

5. CONCLUSION

In conclusion, in this work three biocompatible self-assembly nanoparticles were developed.

In the first chapter, it was observed that DOX-carrying VLPs were interiorized by murine melanoma cells by endocytosis, promoting higher cytotoxicity than pure DOX. This enhanced efficiency on tumor cells treatment is probably related to the autophagy and apoptosis mechanisms triggered by the VLPs, what suggests that DOX-carrying can bring advantages upon conventional treatment with DOX.

In the second chapter, it was observed the complete characterization of decorated VLPs. These constructions could effectively enter two distinct APC cell lines even when different are displayed in their surface. Besides, these platforms promoted an increase in the expression of costimulatory molecules on APCs, suggesting that they can proper present antigens to APCs, what makes them a potential vaccine platform.

In the third chapter, VLPs decorated with the anti-EGFR 7D12 nanobody were developed and this new construction was used to carry DOX. It was observed that the decoration of DOX-loaded particles enhances their cytotoxic effect on colorectal cancer cells that have a mutation related to low responsiveness to chemotherapy, suggesting that this new platform can overcome resistance.

All constructions presented in this thesis exhibit features that put them as possible tools in clinical applications, which is in line with nanotechnology sector tendency, which is invest mostly in the search of new vaccine platforms and alternative technologies applied to cancer treatment.